Computers & Industrial Engineering 185 (2023) 109618

Contents lists available at ScienceDirect

Computers & Industrial Engineering

journal homepage: www.elsevier.com/locate/caie

A novel indicator for sustainability in production planning using Center of Gravity-based assessment of Pareto fronts

Markus Hilbert [a], Andreas Dellnitz [b], Andreas Kleine [a], Madjid Tavana [c,d,*]

[a] Chair of Quantitative Methods, FernUniversität in Hagen, Hagen, Germany
[b] Leibniz-Fachhochschule School of Busines, Hannover, Germany
[c] Business Systems and Analytics Department, Distinguished Chair of Business Analytics, La Salle University, Philadelphia, USA
[d] Business Information Systems Department, Faculty of Business Administration and Economics, University of Paderborn, Paderborn, Germany

ARTICLE INFO

Keywords:
Lot-sizing and scheduling
Performance indicators
Multi-objective optimization
Sustainable manufacturing

ABSTRACT

In sustainable manufacturing, the comparison of different production processes has become increasingly important in recent years due to societal and political demands on companies to obtain a more sustainable business structure. At the shop floor level, production planning based on existing processes is usually approached through mathematical optimization, leading to a Pareto front under multiple conflicting criteria. The decision to exchange production processes then leads to the comparison and evaluation of different Pareto fronts. Here, analyzing the structure of Pareto fronts via performance indicators—such as hypervolume, Euclidean distances, etc.—are often the order of the day. However, respective indicators are often neither easy to communicate to decision-makers nor meaningful regarding economic and environmental impacts when processes are changed. Consequently, we propose a Center of Gravity-based indicator to handle these issues and analyze the efficacy of the proposed method through a bicriteria energy-efficient lot-sizing and scheduling numerical scenario analysis; the conflicting criteria under consideration are electricity costs and indirect emissions. Ultimately, we discuss the selected theoretical properties and approximation features of the proposed concept, and elaborate on the communicational benefits of the new tool.

1. Introduction

Today, sustainability is a key issue forcing companies to achieve a more sustainable business structure, especially due to the societal and political pressure. This is especially true for manufacturing companies, which are responsible for a large portion of global CO2 emissions and have made improving their environmental footprint a top environmental goal (e.g., Li et al., 2022; Tiwari et al., 2015; Wang & Wang, 2022; Wichmann et al., 2019a). As a consequence, the corporate responsibility of manufacturing companies is embedded in the Sustainable Development Goals (SDGs)—like SDG 12 for responsible consumption and production (United Nations (UN), 2015).

In Europe, for example, the Industrial Strategy 2020 calls for companies to move towards more sustainable business models, including the adoption of more resource-efficient processes in particular (EU-COM – European Commission, 2020). However, changing production processes requires a comparison of an existing process with its possible alternatives. For example, a company is considering replacing existing machines with ones that have special features (speed scaling, etc.) or that are probably more resource efficient. To underpin a restructering decision, the assessed alternatives—here, different compositions of machines—must be compared. Typically, in consecutive planning horizons, a company must solve similar production planning problems (i.e., lot-sizing and/or scheduling) at the shop floor level, differing only in the demand to be met. Thus, potential processes to be adopted can be evaluated with respect to the class of planning problems to be solved (e.g., Dong et al., 2016; Liang et al., 2019). In this situation, multi-objective optimization techniques come into play because solving respective planning problems typically involves multiple conflicting criteria such as energy costs and cycle time etc. (e.g., Oukil et al., 2022). The evaluation of different processes then requires the compression and comparison of the Pareto fronts obtained.

* Corresponding author at: Business Systems and Analytics Department, Distinguished Chair of Business Analytics, La Salle University, Philadelphia, PA 19141, United States.
E-mail addresses: markus-andre.hilbert@fernuni-hagen.de (M. Hilbert), andreas.dellnitz@leibniz-fh.de (A. Dellnitz), andreas.kleine@fernuni-hagen.de (A. Kleine), tavana@lasalle.edu (M. Tavana).

https://doi.org/10.1016/j.cie.2023.109618
Received 17 September 2022; Received in revised form 17 April 2023; Accepted 14 September 2023
Available online 10 October 2023

The literature reports several indicators for comparing different Pareto fronts, such as hypervolume ratio, etc. (e.g., Audet et al., 2021). However, a point that is widely neglected is that the result of a Pareto front comparison must ultimately be communicated to a decision-maker so that they can decide to restructure and select the process alternative to be chosen. Therefore, an indicator value must be meaningful and easy-to-interpret, especially concerning economic and ecological statements. For this purpose, we propose a novel Center of Gravity-based (CoG) indicator that allows just this.

In this context, the main research questions of this study are:

- Are the most common Pareto front indicators suitable for communication purposes?
- How can an easy-to-use indicator be designed that enables a meaningful interpretation?
- How does a meaningful indicator support decision-making in a business case?

To answer these questions, we will present and discuss common indicators from the literature with respect to their practicality for a communication purpose. In contrast, our Center of Gravity-based indicator will be put to the test and its weaknesses and remedies will be discussed. The applicability of the novel indicator is then demonstrated using a sustainable bicriteria production planning problem from a metal working company.

The remainder of the article is as follows. Section 2 presents a literature-based and business-related motivation for the proposed approach, followed by the mathematical conceptualization of the new indicator. Selected properties of the novel indicator will be discussed. In Section 3, an energy-efficient bicriteria mixed-integer problem for reducing indirect emissions and electricity costs is developed to show the usefulness of the novel indicator. The indicator is exemplified in a computational study in Section 4. Section 5 concludes this work.

2. Indicators for comparing Pareto fronts

2.1. Motivation for sustainability-driven process comparisons

In past decades, economic criteria such as production costs or tardiness have been the key performance measures in production management (e.g., Maecker & Shen, 2020; Meng et al., 2020). In recent years, however, a paradigm shift has been initiated worldwide, particularly through the growing green movement (e.g., Cui & Lu, 2021; Yenipazarli & Vakharia, 2017). As a result, performance in production is measured not only by the economic result, but also simultaneously by ecological criteria such as indirect carbon emissions (e.g., Alexopoulos et al., 2018; Dong & Ye, 2022; Jaehn, 2016). Accordingly, production planning—lot-sizing and/or scheduling—will be carried out via multicriteria optimization, resulting in Pareto fronts, provided that a conflict of objectives exists (Chen et al., 2020; Copil et al., 2017; T'kindt & Billaut, 2006).

Furthermore, the comparison of production processes in terms of their ecological performance, especially carbon emissions, has received increasing attention in recent years (e.g., Gong & Zhou, 2013).

Now, as motivated in the previous section, the comparison of different processes regarding their sustainability performance—i.e., an economic outcome such as electricity cost and an ecological outcome such as indirect emissions—with respect to the same production planning problem implies the comparison of different Pareto fronts, as depicted in Fig. 1. The literature on comparing different (approximate) Pareto fronts is extensive, but mainly in the context of the performance of metaheuristics (e.g.: Audet et al., 2021; Zitzler et al., 2008; Collette & Siarry, 2004; Riquelme et al., 2015; Zitzler et al., 2003, etc.). Indicators such as S-metric, D-indicators, etc. can be named here, but communication of the result when using an indicator for Pareto front comparison is not considered at all, although this is an essential part of decision support and decision making in business. This is because the design and application of an indicator is primarily considered from an analyst's perspective. However, as empirical research shows, communicating the results cannot be neglected because a decision-maker may lack the mathematical intuition to interpret the results accurately (Hogarth & Soyer, 2015); Fig. 1 illustrates this issue.

To substantiate the need for a new indicator, we will present the essence of the most common indicators in the following.

2.2. Performance indicators in multi-objective optimization

2.2.1. Preliminaries

We now propose studying a production planning problem based on two different production processes. The problem at hand for the two processes can be described via a multicriteria mixed-integer minimization model each.

In general, a multicriteria mixed-integer minimization model can be formulated as follows:

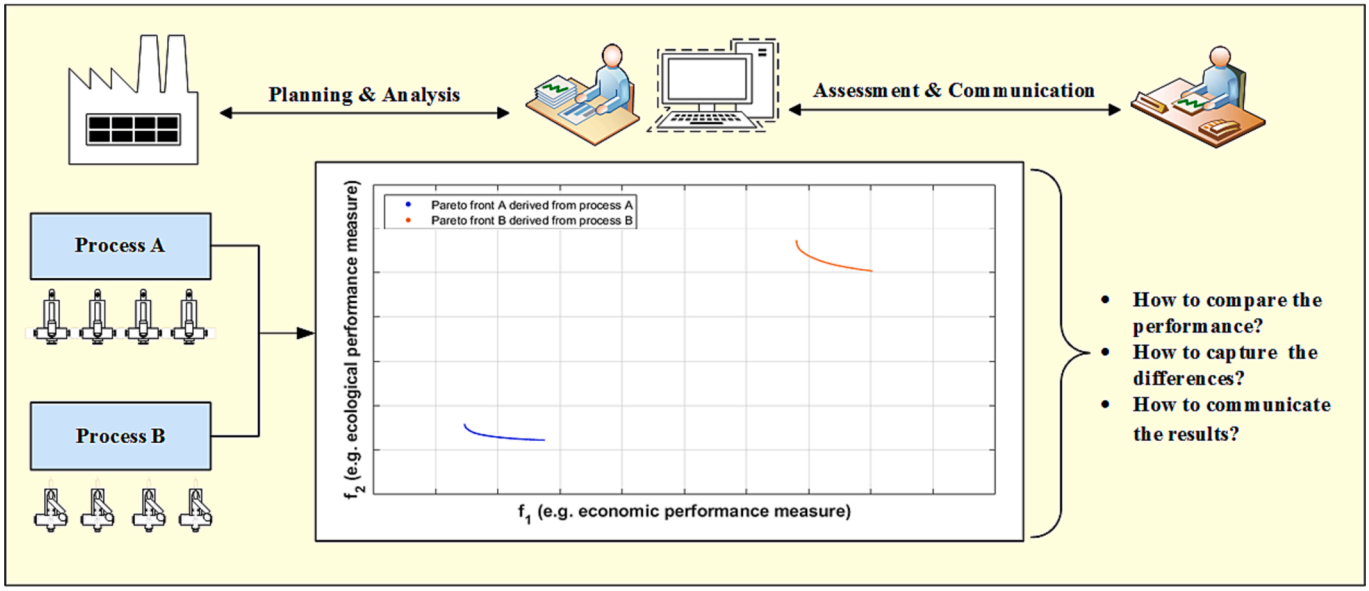

Fig. 1. Assessment and communication of competing processes.

$$\min_{x \in \mathscr{S}} \{f_1(x), \ldots, f_K(x)\} \tag{MP}$$

with $f_k : \mathscr{S} \to \mathbb{R}$, $k \in \{1, \ldots, K\}$ and $K \in \mathbb{N}$, being the objective functions and $\mathscr{S}$ defining the feasible region. In constrained mixed-integer optimization, $\mathscr{S}$ is a subspace of the decision variable space, which will be in the following $\mathbb{R}^{n_1} \times \mathbb{Z}^{n_2}$ with $n_1, n_2 \in \mathbb{N}$ (Kallrath, 2021; Miettinen, 1998). Since processes A and B are similar and involve only a different mix of machine types (for example, throttleable and non-throttleable machines), the corresponding model for a planning problem for each process varies only in its feasible region. Consequently, for processes A and B, we have $\mathscr{S}_A$ and $\mathscr{S}_B$ instead of $\mathscr{S}$ in (MP) with $\mathscr{S}_A \neq \mathscr{S}_B$. We obtain:

$$\min_{x \in \mathscr{S}_A} \{f_1(x), \ldots, f_K(x)\} \tag{MP1}$$

$$\min_{x \in \mathscr{S}_B} \{f_1(x), \ldots, f_K(x)\} \tag{MP2}$$

In single-criterion optimization, differences between two production processes regarding the same planning problem can be revealed by the relation' $\leq$', i.e. we just compare the unique optimal objective function values obtained (Zitzler et al., 2008). However, in a multicriteria setting comprising conflicting objectives, we obtain multiple Pareto-optimal solutions with different degrees of achievement regarding each objective—we obtain a Pareto front instead of a single optimum (Ehrgott, 2005). Consequently, we need to compare two Pareto fronts A and B in the case of two processes A and B, where the first might relate to MP1 and the second to MP2. See Fig. 2 for an illustration of two different Pareto fronts in a bicriteria case. Note that all Pareto fronts presented in this article are discrete; they are finite sets of points.

In this paper, it is sufficient to deal with objective vectors corresponding to a particular solution in the feasible region. Thus, when we mention the Pareto front A, we mean the set A of K-dimensional objective vectors shaping this front. Consequently, we will use concepts—such as Pareto dominance, etc.—solely at the level of the objective space (Zitzler et al., 2003). In this context, Definition 1 clarifies the concept of dominance (Audet et al., 2021).

Definition 1. **(Dominance relations in objective space).** Given two Pareto fronts A and B and $a = (a_1, \ldots, a_K)^\top \in$ A, $b = (b_1, \ldots, b_K)^\top \in$ B. Then,

- $a \preceq b$ (a weakly dominates b) if $a_k \leq b_k \; \forall \; k \in \{1, \ldots, K\}$; i.e., a is not worse than b in all components.
- $a \prec b$ (a dominates b) if $a \preceq b$ and $\exists \; k \in \{1, \ldots, K\}$ such that $a_k < b_k$; i.e., a is not worse than b in all components and better in at least one component.
- A$\preceq$B (A weakly dominates B) if $\forall \; b \in$ B $\exists \; a \in$ A such that $a \preceq b$; i.e., every $b \in$ B is weakly dominated by at least one $a \in$ A. A $\prec$ B (A dominates B) is defined accordingly.

Before presenting the most popular indicators for compressing information on Pareto fronts, we must recall some well-established conventions and definitions.

Assumption 1. Let A and B be two Pareto fronts. Either A$\preceq$B or B$\preceq$A applies.

With Assumption 1, we presuppose that there is a natural order on the set of Pareto fronts. This is typical for performance assessment in multi-objective optimization, and most papers implicitly assume it is fulfilled (Zitzler et al., 2003). In particular, when comparing production processes via Pareto fronts, Assumption 1 is often valid (Weckenborg et al., 2022). However, with Assumption 1, we get the following:

Definition 2. If A$\preceq$B and A $\neq$ B, then A is called better than B, abbreviated A$\triangleright$B.

There are many indicator-based concepts for measuring the goodness or quality of Pareto front approximations (Audet et al., 2021; Collette & Siarry, 2004; Riquelme et al., 2015; Wang et al., 2022; Zitzler et al., 2008). They lead to more precise quantitative statements instead of qualifying via A$\triangleright$B only. More precisely, a quality indicator is a mapping of a Pareto front approximation to a real value (Zitzler et al., 2008). Such indicators (especially *convergence* indicators) quantify the distance between two sets of points in objective space, allowing a statement on the advantageousness between different approximation algorithms (Audet et al., 2021; Deb & Jain, 2004; Riquelme et al., 2015).

In principle, these distance-based concepts might also be suitable for technology comparisons. However, we aim to compare *exact* Pareto fronts and not the performance of approximation algorithms. Therefore, we prefer the notion of the *comparative indicator*:

Definition 3. **(Binary vector-valued comparative indicator).** Let Ψ be a set containing different Pareto fronts. A binary vector-valued comparative indicator is a relation $I : \Psi \times \Psi \to \mathbb{R}^d$ with $d \in \mathbb{N}$, which assigns a real numbered d-dimensional vector to two exact Pareto fronts.

For $d = 1$, the indicator assigns a single real number. Since the indicator serves as an information tool for a decision-maker, however, it may be practical to embed several types of information in a d-tuple (Deb & Jain, 2004; Zitzler et al., 2003).

A very important transitivity property of a comparative indicator should be as follows:

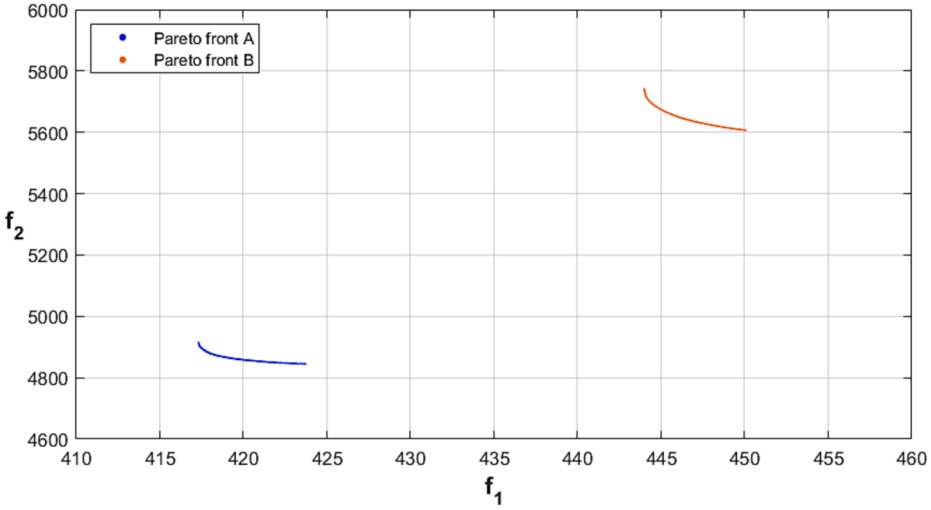

Fig. 2. Exemplary Pareto fronts in two-dimensional space.

Definition 4. (Comparative monotonicity). Let A⪯B as well as B⪯C for three Pareto fronts $A, B, C \in \Psi$. Then, A⪯C and $I(A, B) \leq I(A, C)$.

Definition 4 means that the natural order on the set of Pareto fronts, if any, should be reflected by the indicator.

In summary, a comparative indicator should reveal the (dis-)advantageousness of processes and adequately support the decision-making process. Since the communication of respective results to a decision-maker is an essential step in this process, in the next sections, we will present classical indicators and discuss their informative value with respect to such a purpose.

2.2.2. Performance indicators

Let A, B be two Pareto fronts, where $a \in A$ is an element of A with $a = (a_1, \ldots, a_K)^\top$, a_k being the k-th component corresponding to the k-th objective; this also applies analogously to $b \in B$. Furthermore, we assume A ⪯ B. Next, we present popular indicators used in the literature but adapted to the notion of binary comparative indicators.

- **Generational Distance and Inverted Generational Distance (I_{GD} and I_{IGD}):**

The Generational Distance and Inverted Generational Distance, respectively, are given by

$$I_{GD}(A, B) = \frac{1}{|B|}\left(\sum_{b\in B} \min_{a\in A} \|b-a\|_2^p\right)^{\frac{1}{p}}, \tag{1}$$

$$I_{IGD}(A, B) = I_{GD}(B, A). \tag{2}$$

With $p = 1$, I_{GD} measures the averaged minimal Euclidean distance between every point of Pareto front B and its nearest neighbor of Pareto front A. I_{IGD} is defined accordingly, except that A and B are swapped, see Eq. (2) (Coello & Cortés, 2005; Van Veldhuizen, 1999).

- ***D* Indicator family (I_{D1} and I_{D2}):**

The D indicators I_{D1} and I_{D2} are somewhat similar to I_{GD} or I_{IGD}: they measure the average and worst-case component-wise distance in objective space, respectively (Zitzler et al., 2008). The indicators are defined by eqs. (3, 4) (Czyżak & Jaszkiewicz, 1998).

$$I_{D1}(A, B) = \frac{1}{|A|}\left(\sum_{a\in A} \min_{b\in B} \max_{1\leq k\leq K} \{0, w_k(b_k - a_k)\}\right) \tag{3}$$

$$I_{D2}(A, B) = \max_{a\in A} \min_{b\in B} \max_{1\leq k\leq K} \{0, w_k(b_k - a_k)\} \tag{4}$$

In general, the weights form a convex combination, i.e. $\sum_k w_k = 1$ and $w_k \geq 0 \ \forall \ k$. En equal weighting $w_1 = \ldots = w_K = \frac{1}{K}$ is a common specification.

- **Binary multiplicative epsilon indicator (I_ϵ):**

The epsilon indicator equals the minimal factor ϵ by which each objective vector of A must be multiplied such that the resulting transformed Pareto front becomes weakly dominated by front B:

$$I_\epsilon(A, B) = \inf_{\epsilon\in\mathbb{R}} \{\forall a \in A \ \exists \ b \in B : b \preceq_\epsilon a\}, \tag{5}$$

where $\preceq_\epsilon$ denotes the ϵ-dominance relation: $b \preceq_\epsilon a \Leftrightarrow \forall k : b_k \leq \epsilon \cdot a_k$ (Zitzler et al., 2008).

- **Hypervolume Ratio ($I_{HV}^{z^*}$):**

The hypervolume (S-metric)—one of the most widely used indicators— yields the volume of the K-dimensional objective space, which is weakly dominated by a set of points bounded by a reference point $z^* \in \mathbb{R}^K$ and thus strongly depends on the chosen reference point (Zitzler and Thiele (1998); Audet et al., 2021). The unary hypervolume indicator is given by

$$HV_{z^*}(A) = \lambda_K\left(\bigcup_{a\in A}(a, z^*]\right), \tag{6}$$

where λ_K is the K-dimensional Lebesque measure. However, to compare two Pareto fronts, the binary hypervolume ratio is often used, see Eq. (7) (Collette & Siarry, 2004):

$$I_{HV}^{z^*}(A, B) = \frac{HV_{z^*}(B)}{HV_{z^*}(A)} \tag{7}$$

Note here that the volumes covered by fronts A and B are calculated using the same reference point z^*. The nadir point (plus an arbitrarily small vector $\varepsilon > 0$) of the dominated front B, $z_B^{nad} + \varepsilon$, is a common choice for z^* due to Assumption 1 (Knowles & Come, 2002; Lewis et al., 2008).

The following Table 1 summarizes the indicators presented so far and their outcome with respect to Fig. 2. In general, the indicators are in principle suitable for comparing Pareto fronts (Audet et al., 2021; Riquelme et al., 2015). From a decision-maker's point of view, however, it is questionable whether the values of the indicators are interpretable when analyzing changes in production processes.

Consider the two Pareto fronts shown in Fig. 2, each resulting from

Table 1
Summary of presented indicators with application to Fig. 2.

Indicator	Formula	Note	Value
I_{GD}	$I_{GD}(A, B) = \frac{1}{\lvert B\rvert}\left(\sum_{b\in B} \min_{a\in A} \lVert b-a\rVert_2^p\right)^{\frac{1}{p}}$	$p = 2$ for computational simplification	26.0207
I_{IGD}	$I_{IGD}(A, B) = \frac{1}{\lvert A\rvert}\left(\sum_{a\in A} \min_{b\in B} \lVert b-a\rVert_2^p\right)^{\frac{1}{p}}$	$p = 2$ for computational simplification	38.1952
I_{D1}	$I_{D1}(A, B) = \frac{1}{\lvert A\rvert}\left(\sum_{a\in A} \min_{b\in B} \max_{1\leq k\leq K} \{0, w_k(b_k - a_k)\}\right)$	$w_1 = \ldots = w_K = \frac{1}{K}$	365.9067
I_{D2}	$I_{D2}(A, B) = \max_{a\in A} \min_{b\in B} \max_{1\leq k\leq K} \{0, w_k(b_k - a_k)\}$	$w_1 = \ldots = w_K = \frac{1}{K}$	380.7864
I_ϵ	$I_\epsilon(A, B) = \inf_{\epsilon\in\mathbb{R}} \{\forall a \in A \exists b \in B : b \preceq_\epsilon a\}$	–	1.1572
$I_{HV}^{z^*}$	$I_{HV}^{z^*}(A, B) = \frac{\lambda_K\left(\bigcup_{b\in B}(b, z^*]\right)}{\lambda_K\left(\bigcup_{a\in A}(a, z^*]\right)}$	$z^* = z_B^{nad} + \begin{pmatrix} 0.0001 \\ \ldots \\ 0.0001 \end{pmatrix}$	0.0209

solving a production planning problem that considers either Process A or Process B. But how can these values in Table 1 be interpreted to draw business implications, and how can these implications be communicated to a decision-maker as a key performance indicator? The indicators $I_{GD}(\mathrm{A},\mathrm{B})$, $I_{IGD}(\mathrm{A},\mathrm{B})$ and $I_{D1}(\mathrm{A},\mathrm{B})$ as well as $I_{D2}(\mathrm{A},\mathrm{B})$ show the compressed distances between the two fronts; the ϵ-indicator implies that Pareto front A can be multiplied by approximately 1.16 before it becomes dominated by Pareto front B. From all these numbers, we learn that Pareto front A dominates Pareto front B, and as a consequence, A$\triangleright$B. However, this conclusion can also be drawn by visual inspection of Fig. 2. The same holds true for the Hypervolume Ratio $I^{\frac{z}{HV}}_{HV}(\mathrm{A},\mathrm{B})$ because the hypervolume of Pareto front B covers approximately 2% of the hypervolume of Pareto front A. However, concrete economic or ecological implications—such as efficiency rates, etc.—can hardly be derived from these numbers, especially not for a decision-maker. Therefore, we propose a new indicator designed for such a communication purpose in the next section.

2.3. A Center of Gravity-based indicator

The indicators presented so far give some idea of how two Pareto fronts differ from each other, but without characterizing the gain or loss in terms of the objective functions in an intelligible way. Second, the indicators are quite computationally expensive. For example, the costs for computing the Hypervolume Ratio are exponential in the number of objectives (Dyer & Frieze, 1988; Zitzler et al., 2008). Therefore, we propose a novel indicator based on the Center of Gravity (CoG) of a Pareto front to obtain a more tangible and less computationally expensive instrument. Figs. 3 and 4 show the essence of the idea in a bicriteria setting.

Obviously, the CoG is given by the arithmetic mean of each component of the points of a Pareto front; the following definition provides the calculation of the CoG.

Definition 5. (Center of Gravity (CoG)). Let $\mathrm{A} \in \Psi$ be a Pareto front with $a_l = \left(a^l_1, \ldots, a^l_K\right)^\top \in \mathbb{R}^K$ being the points of A for $l = 1, \ldots, |\mathrm{A}|$. The CoG of A is now given by

$$f_{CoG}(\mathrm{A}) = \left(\frac{1}{|\mathrm{A}|}\sum_{l=1}^{|\mathrm{A}|} a^l_1, \ldots, \frac{1}{|\mathrm{A}|}\sum_{l=1}^{|\mathrm{A}|} a^l_K\right)^\top. \tag{8}$$

Based on the CoGs of both Pareto fronts A and B, the deviation in percent is easy to assess, see again Fig. 4. The new binary CoG-based indicator then reads

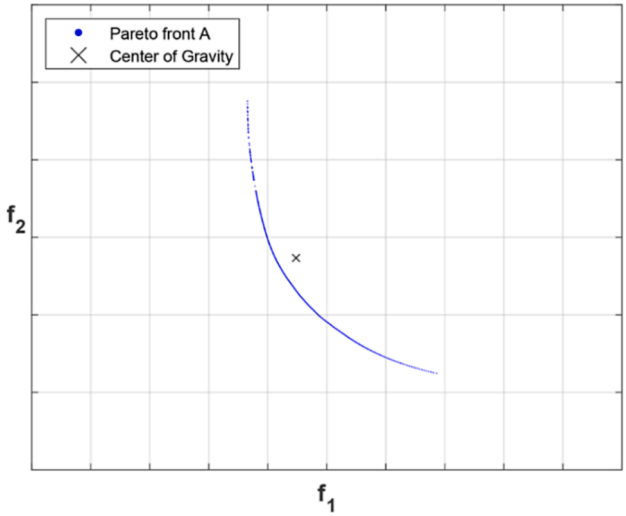

Fig. 3. Center of Gravity of a Pareto front.

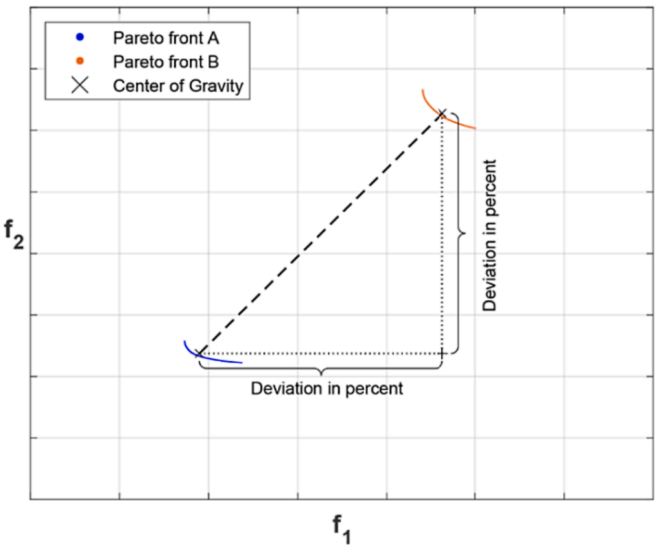

Fig. 4. Center of Gravity-based deviations.

$$I_{CoG}(\mathrm{A},\mathrm{B}) = 1 - \mathbf{w}^\top\left(f_{CoG}(\mathrm{A}) \circ \widehat{f_{CoG}(\mathrm{B})}\right), \tag{9}$$

where $\widehat{f_{CoG}(\mathrm{B})}$ is the Hadamard inverse of $f_{CoG}(\mathrm{B})$, i.e., the component-wise vector inversion, and $f_{CoG}(\mathrm{A}) \circ \widehat{f_{CoG}(\mathrm{B})}$ is the Hadamard product, i.e., the component-wise vector multiplication. Here, we assume that $\mathrm{A} \preceq \mathrm{B}, \mathrm{A} \neq \mathrm{B}$ and $f_{CoG}(\mathrm{B}) \neq (0, \ldots, 0)^\top$ such that the Hadamard inverse $\widehat{f_{CoG}(\mathrm{B})}$ of $f_{CoG}(\mathrm{B})$ is well defined. Furthermore, the weights $\mathbf{w}^\top = (w_1, \ldots, w_K)$ must be specified a priori and should meet $\sum_k w_k = 1$ with $w_k \geq 0 \ \forall\ k$. Then, $I_{CoG}(\mathrm{A},\mathrm{B})$ provides the weighted average relative improvement potential regarding each objective when altering the processes from B to A.

However, it is also possible to decompose the new indicator to formulate an unweighted version of $I_{CoG}(\mathrm{A},\mathrm{B})$, which then provides the average relative improvement potential for each objective. The component-wise version reads:

$$I^{comp}_{CoG}(\mathrm{A},\mathrm{B}) = \overrightarrow{1} - \left(f_{CoG}(\mathrm{A}) \circ \widehat{f_{CoG}(\mathrm{B})}\right). \tag{10}$$

Note here that $I^{comp}_{CoG}(\mathrm{A},\mathrm{B})$ is a K-tuple instead of a single number as obtained with (9) and $\overrightarrow{1}$ a vector of ones. In addition, I_{CoG} can be obtained by computing the weighted sum of the tuple obtained by (10).

About our numerical example (Fig. 2), Table 2 compares the values of the presented indicators. Using I_{CoG} with $w_1 = w_2 = \frac{1}{2}$, we now obtain the following contextual statement: Changing the processes from B to A concerning the underlying planning problem can reduce the equally weighted achievement of both production objectives by about 10% on average. Applying I^{comp}_{CoG}, we obtain the statement that the average achievement of the first objective can be reduced by about 6% and that of the second by about 14%.

Alltogether, due to the following main features, $I_{CoG}(\mathrm{A},\mathrm{B})$ is beneficial compared to the other presented indicators:

a. $I_{CoG}(\mathrm{A},\mathrm{B})$ has a clear meaning: If $I_{CoG}(\mathrm{A},\mathrm{B}) = q \geq 0$ (< 0), then technology A improves (worsens) our outcomes by q percent on average compared to B.
b. From a computational point of view, its calculation is only proportional to the elements of the two Pareto fronts.
c. $I_{CoG}(\mathrm{A},\mathrm{B})$ can just as easily be used for higher dimensions, i.e. $K > 2$, and still retains its basic informative value.
d. A component-by-component version of $I_{CoG}(\mathrm{A},\mathrm{B})$ can be easily obtained and will retain all of the features of $I_{CoG}(\mathrm{A},\mathrm{B})$.

Table 2
Indicator values with respect to Fig. 2.

I_{GD}	I_{IGD}	I_{D1}	I_{D2}	I_{ϵ}	I_{HV}^{-}	I_{CoG}	I_{CoG}^{comp}
26.0207	38.1952	365.9067	380.7864	1.1572	0.0209	0.0998	$(0.0611, 0.1384)^{\top}$

e. $I_{CoG}(\mathrm{A},\mathrm{B})$ can be easily approximated a priori, which reduces the computational effort enormously; for more information on this subject, refer to Section 4.3.

The next section illuminates some properties of $I_{CoG}(\mathrm{A},\mathrm{B})$.

2.4. Selected properties of I_{CoG}

When we introduced $I_{CoG}(\mathrm{A},\mathrm{B})$ in Fig. 4 (or see Fig. 2 as well), we assumed that A$\preceq$B given two Pareto fronts A and B. However, the calculated Pareto fronts in Fig. 4 (or Fig. 2) have a stronger relationship than just A $\preceq$ B. It applied that every point of Pareto front A weakly dominates every point of Pareto front B. We call this relation *weakly total dominance:*

Definition 6. (Weakly total dominance). Given Pareto fronts A and B, then A weakly totally dominates B if for every $a \in \mathrm{A}$ it holds that $a \preceq b \forall b \in \mathrm{B}$.

Note that Definition 6 also implies A$\preceq$ B and A$\neq$ B. If Definition 6 does not apply to A and B, caution is advised when drawing implications from I_{CoG}. Three possible cases are demonstrated:

- **1st case: overlapping CoGs:**

Fig. 5 visualizes two Pareto fronts A, B with overlapping CoGs. In this case, $I_{CoG}(\mathrm{A},\mathrm{B}) = 0$. When drawing implications from this—without a visual inspection—, it might be assumed that both process A and process B are equally good at carrying out an underlying production plan. However, A$\preceq$B and A $\neq$ B, following that A$\triangleright$B according to Definition 2.

- **2nd case: reversed ordered CoGs:**

Here, the CoG of the dominated front B is smaller than the CoG of A, see Fig. 6; this implies $I_{CoG}(\mathrm{A},\mathrm{B}) < 0$ and thus a misclassification of the performance of the processes because A$\triangleright$B.

- **3rd case: unorderable CoGs:**

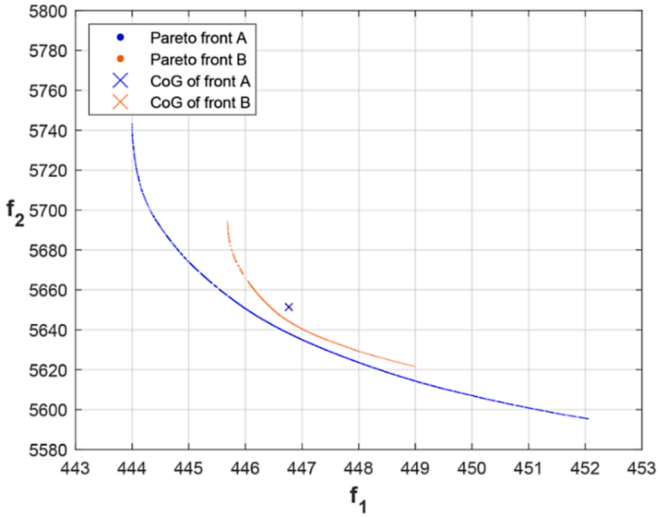

Fig. 5. Overlapping CoGs.

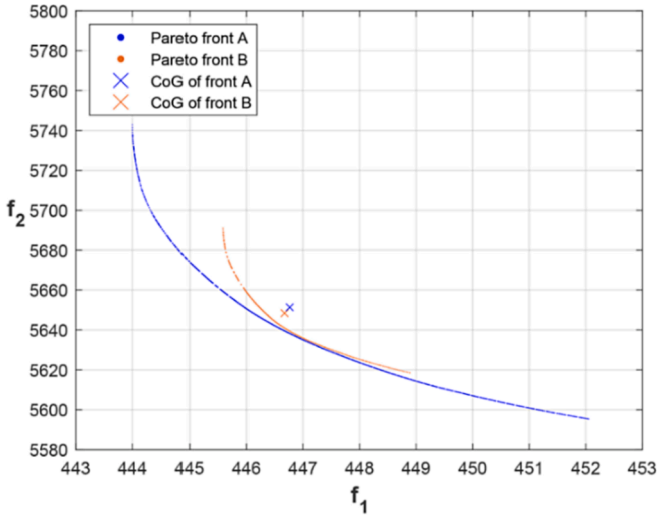

Fig. 6. Reversed order.

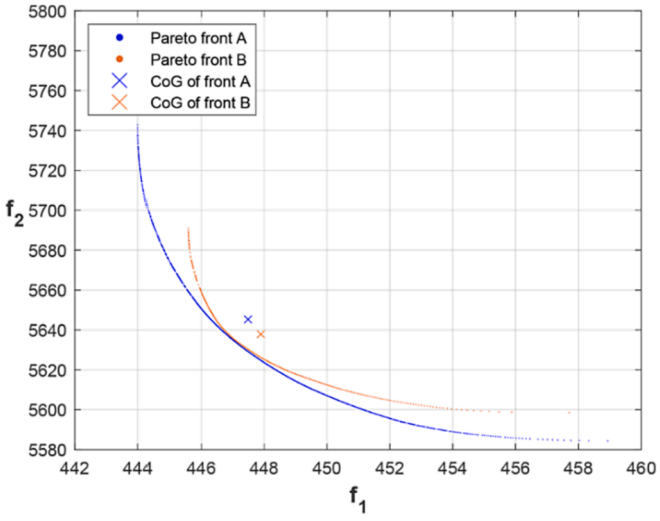

Fig. 7. Unorderable CoGs.

In Fig. 7, both CoGs are unorderable, i.e. $f_{CoG}(\mathrm{A}) \leq f_{CoG}(\mathrm{B})$ does not hold or vice versa; here, $I_{CoG}(\mathrm{A},\mathrm{B}) < 0$. This again misclassifies the performance because A$\triangleright$B.

The above examples show that, in some cases, the natural order on the Pareto fronts remains unrevealed when calculating the I_{CoG} without any further treatment. Additionally, I_{CoG} might show non-monotonic behavior—the same applies to the other indicators except the unary hypervolume indicator (Zitzler et al., 2008)—as illustrated in Fig. 8. Here, one can observe A$\preceq$B and $B \preceq C$ but $I_{CoG}(\mathrm{A},\mathrm{B}) > I_{CoG}(\mathrm{A},\mathrm{C})$. However, this monotonicity property is always satisfied if Pareto front A weakly totally dominates Pareto front B and Pareto front B weakly totally dominates Pareto front C; the following Lemma 1 and Theorem 1 specify this assertion.

Lemma 1. *Let A, B be two Pareto fronts in* K*-dimensional space* $\mathbb{R}^{\mathrm{K}}$*, with* $A \preceq B$ *and* $A \neq B$*. If every point of A weakly dominates every point of B, then it*

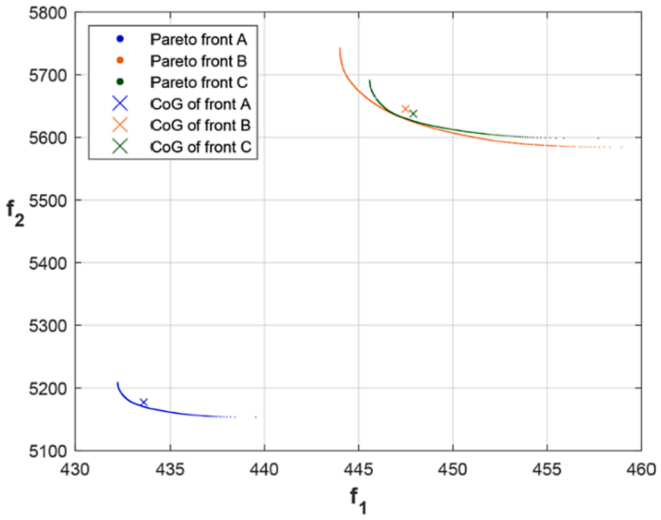

Fig. 8. Non-monotonic behavior of I_{CoG}.

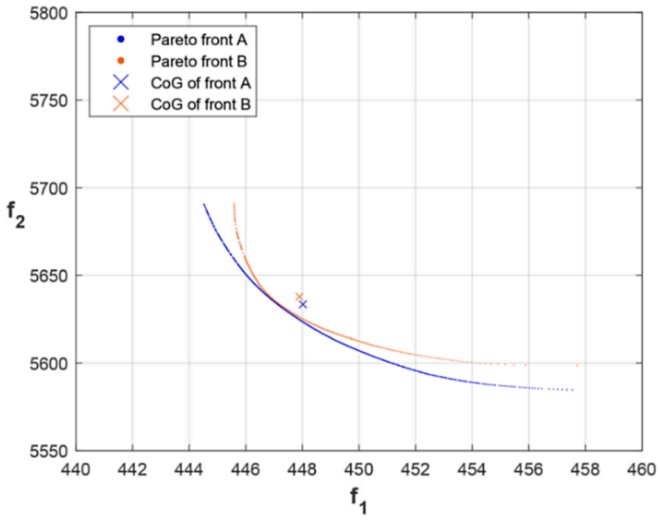

Fig. 9. Minimally pruned front.

holds that $f_{CoG}(A) \leq f_{CoG}(B)$.

Proof:

Given that A weakly totally dominates B. Let $a^{nadir} = \left(a_1^{nadir}, \ldots, a_K^{nadir}\right)^\top \in \mathbb{R}^K$ be the nadir point of Pareto front A. It then holds that a^{nadir} weakly dominates every point of B.

Assume that this does not hold. Then, there exists a point $b \in$ B that is not weakly dominated by a^{nadir}. It follows that one of the K components of a^{nadir} is greater than the respective component of point b, which contradicts the assumption that every point of A weakly dominates every point of B. Consequently, a^{nadir} weakly dominates every point of B. We then have

$$f_{CoG}(\mathrm{B}) = \left(\frac{1}{|\mathrm{B}|}\sum_{l=1}^{|\mathrm{B}|} b_1^l, \ldots, \frac{1}{|\mathrm{B}|}\sum_{l=1}^{|\mathrm{B}|} b_K^l\right)^\top \geq \left(\frac{1}{|\mathrm{B}|}\sum_{l=1}^{|\mathrm{B}|} a_1^{nadir}, \ldots, \frac{1}{|\mathrm{B}|}\sum_{l=1}^{|\mathrm{B}|} a_K^{nadir}\right)^\top$$
$$\geq \left(a_1^{nadir}, \ldots, a_K^{nadir}\right)^\top \geq f_{CoG}(\mathrm{A}),$$

where b^l are the points of B, with $l = 1, \ldots, |\mathrm{B}|$. This completes the proof. □

Based on this lemma, we propose:

Theorem 1. **(Qualification criterion for monotony (QC)).** *Let* A, B *and* C *be three Pareto fronts in K-dimensional space* $\mathbb{R}^K$ *with* A⪯B⪯C *and* $\mathrm{A} \neq \mathrm{B} \neq \mathrm{C}$. *If it holds that* A *weakly totally dominates* B *as well as* B *weakly totally dominates* C, *then* $I_{CoG}(\mathrm{A}, \mathrm{B}) \leq I_{CoG}(\mathrm{A}, \mathrm{C})$.

Proof:

Due to Lemma 1 $f_{CoG}(\mathrm{A}) \leq f_{CoG}(\mathrm{B}) \leq f_{CoG}(\mathrm{C})$ holds, and the statement follows immediately. □

The new indicator should reflect the natural ordering of ordered Pareto fronts; if A does not weakly totally dominate B, however, the indicator may not meet this feature. Therefore, we propose two approaches to remedy this flaw. The gist of both procedures is the pruning of a front in order to meet the aforementioned property. The first approach relies on the following definition:

Definition 7. **(Minimally pruned front).** Let A, and B be two Pareto fronts in K-dimensional space $\mathbb{R}^K$ and A⪯B. The set $\widetilde{\mathrm{A}} = \{a \in \mathrm{A} \mid \exists\, b \in \mathrm{B}$ with $a \preceq b\}$, $\widetilde{\mathrm{A}} \preceq$ B, is called the minimally pruned front, i.e., the maximal subset $\widetilde{\mathrm{A}}$ of A that weakly dominates front B.

The second pruning is based on a minimum Euclidean distance:

Definition 8. **(Euclidean-pruned front).** Let A, B be two Pareto fronts in K-dimensional space $\mathbb{R}^K$ and A⪯B. The multiset $\widehat{\mathrm{A}}$, with $|\widehat{\mathrm{A}}| = |\mathrm{B}|$ and $\widehat{\mathrm{A}} \preceq$ B, is called the Euclidean-pruned front if the following holds: Every point $a^l \in \widehat{\mathrm{A}}$ is a solution of $\underset{a \in \mathrm{A}, a \preceq b^l}{\operatorname{argmin}} \left\|a - b^l\right\|_2$ for $b^l \in \mathrm{B}$, $l = 1, \ldots, |\mathrm{B}|$.

The latter definition states that every point of $\widehat{\mathrm{A}}$ weakly dominates (at least) one point of B and has minimal Euclidean distance to this point

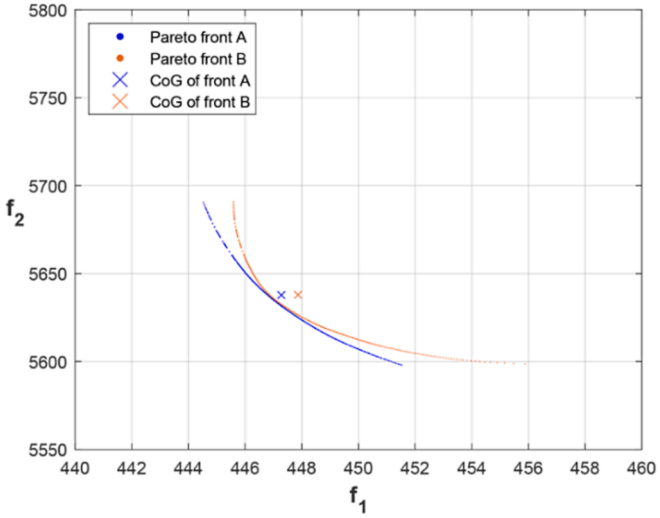

Fig. 10. Euclidean-pruned front.

compared to the other points of A which also weakly dominate this point of B. Note there that $\widehat{\mathrm{A}}$ is a multiset with the same cardinality as B. Of course, metrics other than the Euclidean metric can be used in Definition 8; the differences in the pruning of a front may be a topic for future research.

Based on the two Pareto fronts given in Fig. 7, Fig. 9 and Fig. 10 illustrate the philosophies of the two definitions.

A minimally pruned front—for example, as in Fig. 9—seems to be appealing because fewer points of Pareto front A may be deleted in contrast to the Euclidean-based version. Furthermore, if Pareto front A weakly totally dominates front B, then $I_{CoG}\left(\widetilde{\mathrm{A}},\mathrm{B}\right)$ and $I_{CoG}(\mathrm{A},\mathrm{B})$ coincide; see Proposition 1.

Proposition 1. *Let A, B be two Pareto fronts in* K*-dimensional space $\mathbb{R}^{\mathrm{K}}$. If Pareto front A weakly totally dominates front B, then $I_{CoG}(A,B) = I_{CoG}\left(\widetilde{A},B\right)$.*

Proof:

$\widetilde{\mathrm{A}} = \mathrm{A}$ since A weakly totally dominates B. Consequently, $I_{CoG}\left(\widetilde{\mathrm{A}},\mathrm{B}\right) = I_{CoG}(\mathrm{A},\mathrm{B})$. □

As can be seen in Fig. 9, however, a minimally pruned front does not prevent the 3rd case of unorderable CoGs. To remedy this deficit, we have developed the concept of a Euclidean-pruned front. The following theorem provides the corresponding result:

Theorem 2. *Let A, B be two Pareto fronts in K-dimensional space $\mathbb{R}^K$, with $A \preceq B$ and $\widehat{A}$ being the Euclidean-pruned front of A with respect to B. Then, we have $f_{CoG}(\widehat{A}) \leq f_{CoG}(B)$ and, additionally, we get $I_{CoG}(\widehat{A},B) > 0$ if $A \neq B$ and $w_1,\ldots,w_K > 0$.*

Proof:

The points of Pareto front B are denoted by $b^1,\ldots,b^{|\mathrm{B}|}$ and $\widehat{a}^1,\ldots,\widehat{a}^{|\mathrm{B}|}$ for $\widehat{\mathrm{A}}$, respectively. Please note, $|\widehat{\mathrm{A}}| = |\mathrm{B}|$ according to the definition of a Euclidean-pruned front.

Due to Definition 8, the following holds: $\forall b^l \in \mathrm{B}\ (l = 1,\ldots,|\mathrm{B}|)\ \exists\ \widehat{a} \in \widehat{\mathrm{A}}$ such that

$\widehat{a} \preceq b^l$. Now, we sort the points $\widehat{a}^1 \preceq b^1, \widehat{a}^2 \preceq b^2, \ldots, \widehat{a}^{|\mathrm{B}|} \preceq b^{|\mathrm{B}|}$ accordingly. Then, we have

$$f_{CoG}(\mathrm{B}) = \left(\frac{1}{|\mathrm{B}|}\sum_{l=1}^{|\mathrm{B}|} b_1^l,\ldots,\frac{1}{|\mathrm{B}|}\sum_{l=1}^{|\mathrm{B}|} b_K^l\right)^{\top} \geq \left(\frac{1}{|\mathrm{B}|}\sum_{l=1}^{|\mathrm{B}|} \widehat{a}_1^l,\ldots,\frac{1}{|\mathrm{B}|}\sum_{l=1}^{|\mathrm{B}|} \widehat{a}_K^l\right)^{\top} = f_{CoG}(\mathrm{A}).$$

This shows $f_{CoG}(B) \geq f_{CoG}(\widehat{A})$.

The second part of the theorem is that if $\mathrm{A} \neq \mathrm{B}$, then $I_{CoG}(\widehat{\mathrm{A}},\mathrm{B}) > 0$, applying positive weights $w_1,\ldots,w_K > 0$.

Because of $\mathrm{A} \neq \mathrm{B}$, there exist at least one index l such that $\widehat{a}^l \preceq b^l$ and $\left\|\widehat{a}^l - b^l\right\|_2 > 0$. Consequently, $\widehat{a}^l$ is at least strictly smaller in one component than b^l. It follows that $I_{CoG}(\widehat{\mathrm{A}},\mathrm{B})$ is at least strictly smaller in one component than $f_{CoG}(\mathrm{A},\mathrm{B})$, which completes the proof. □

Still, the conformity with the monotonicity property as described in Definition 4 is not yet guaranteed due to the sequence dependency when pruning Pareto fronts. Therefore, we present the concept of *conditional monotonicity*; it is a direct consequence of Theorem 2.

Corollary 1. **(Conditional monotonicity).** *Let* $\mathrm{A},\mathrm{B},\mathrm{C}$ *be three Pareto fronts, with* $\mathrm{A} \preceq \mathrm{B} \preceq \mathrm{C}$*, with* $\widehat{\mathrm{B}}$ *being the Euclidean-pruned front of* B *with respect to* C*, and* $\widehat{\widehat{\mathrm{A}}}$ *being the Euclidean-pruned front of* A *with respect to* $\widehat{\mathrm{B}}$*, then it holds that* $I_{CoG}(\widehat{\widehat{\mathrm{A}}},\widehat{\mathrm{B}}) \leq I_{CoG}(\widehat{\mathrm{B}},\mathrm{C})$.

Proof:

Due to Theorem 2, $f_{CoG}(\widehat{\widehat{\mathrm{A}}}) \leq f_{CoG}(\widehat{\mathrm{B}}) \leq f_{CoG}(\mathrm{C})$ applies and the assertion follows from it. □

However, a possible drawback of the second approach might be found in the following fact: If A weakly totally dominates B, then the Euclidean-pruned front of A is a multiset containing |B| times the same point of A. Hence, $I_{CoG}(\widehat{\mathrm{A}},\mathrm{B})$ underestimates the average improvement between A and B given by $I_{CoG}(\mathrm{A},\mathrm{B})$. Consequently, an analyst should apply and check the triplet $I_{CoG}(\mathrm{A},\mathrm{B})$, $I_{CoG}\left(\widetilde{\mathrm{A}},\mathrm{B}\right)$ and $I_{CoG}(\widehat{\mathrm{A}},\mathrm{B})$, as demonstrated in Table 3 for selected scenarios.

A possible interpretation of the triplet when Assumption 1 holds is presented in Table 4, where the third component—the Euclidean-pruned variant—serves as a first signal component: If it is positive, then A▷B. The smallest positive component of the triplet is then used as a communication vehicle, which informs about the smallest average relative improvement potential. Otherwise, if $I_{CoG}(\widehat{\mathrm{A}},\mathrm{B}) < 0$, the highest average relative deterioration potential charaterizes the situation. This reading is therefore a kind of prudence principle.

With Table 4 at hand, Table 3 then reads as follows: In the first row—the case of overlapping CoGs—, we see that $I_{CoG}(\widehat{\mathrm{A}},\mathrm{B}) > 0$ and therefore A▷B; $I_{CoG}(\mathrm{A},\mathrm{B}) = 0$ does not reflect this order. Because the second component is the smallest positive component, $I_{CoG}\left(\widetilde{\mathrm{A}},\mathrm{B}\right) = 0.0006$, we use this component for interpretation. The interpretation of that scenario is then as follows: The pessimistic average weighted performance can be improved on average by 0.06% by changing the processes from B to A. The interpretation of the second and third row of Table 3 is accordingly.

The next section demonstrates the applicability of the novel indicator for a production-related planning problem.

Table 3
Exemplification of the information triplet.

Scenarios	$\left(I_{CoG}(\mathrm{A},\mathrm{B}),I_{CoG}(\widetilde{\mathrm{A}},\mathrm{B}),I_{CoG}(\widehat{\mathrm{A}},\mathrm{B})\right)$
Pareto fronts A and B in Fig. 5, $w_1 = w_2 = \frac{1}{2}$	$(0.0000, 0.0006, 0.0007)$
Pareto fronts A and B in Fig. 6, $w_1 = w_2 = \frac{1}{2}$	$(-0.0004, 0.0003, 0.0004)$
Pareto fronts A and B in Fig. 7, $w_1 = w_2 = \frac{1}{2}$	$(-0.0002, 0.0002, 0.0007)$

Table 4
Prudent interpretation of the information triplet.

Signaling component	Interpretation component
$I_{CoG}(\widehat{\mathrm{A}},\mathrm{B}) > 0 \rightsquigarrow \mathrm{A} \triangleright \mathrm{B}$	Smallest positive component of the triplet
$I_{CoG}(\widehat{\mathrm{A}},\mathrm{B}) < 0 \rightsquigarrow \mathrm{B} \triangleright \mathrm{A}$	Smallest negative component of the triplet

3. Sustainable bicriteria lot-sizing and scheduling

3.1. Brief literature review on energy-efficient production planning

In the following, we analyze an energy-efficient bicriteria single-stage parallel machine production planning problem to demonstrate the usefulness of the indicator I_{CoG}. A practical justification for such planning problems is provided, for example, by Anghinolfi et al. (2021) or Moon et al. (2013).

In the Energy Efficient Production Planning (EEPP) literature, studying trade-offs between electricity costs under price-dynamic electricity tariffs (Bänsch et al., 2021) and classical criteria, like cycle time or total tardiness (e.g., Ding et al., 2021; Ho et al., 2022), is often the credo. To leverage electricity costs in such an environment, one can make use of the power-down approach and/or speed scaling (Biel & Glock, 2016; Ding et al., 2016; Liu & Huang, 2014; Luo et al., 2013; Mansouri et al., 2016; Schulz et al., 2020 and Wichmann et al., 2019b). Likewise, flexibility of manufacturing systems can be captured by

variable machine states (e.g. 'on', 'off', etc.) and/or different production speed levels and/or the embedding of parallel machines with different power requirements (Dellnitz et al., 2020; Giglio et al., 2017; Wang et al., 2022).

While electricity costs is a well-established performance measure in EEPP, indirect carbon emissions are less frequently addressed in the literature, even though they are an inherent part of Scope 2 of the GHG Protocol. (https://ghgprotocol.org). Several articles address this issue in the literature, but with different philosophies; cf. Ding et al. (2016), Gu et al. (2021) and Dellnitz et al. (2020). In such analyses, time-of-use electricity tariffs are the order of the day (Schulz & Linß, 2020; Zhang et al., 2014; Holland & Mansur, 2008), and real-time pricing is less frequently considered (Dellnitz et al., 2020).

Therefore, motivated by the literature related to EEPP, we will study the trade-offs between electricity costs and indirect emissions in the presence of a real-time pricing electricity tariff. To exploit system flexibiliy, a power-down and speed scaling approach in a parallel machine environment is taken into account. For a more detailed literature overviews on the above subjects, see Bänsch et al. (2021), Gahm et al. (2016), and Neufeld et al. (2022).

3.2. Problem description

We now investigate an application of the new indicator based on a production planning problem at the shop floor level from a metal-working company, which can be described via a bicriteria mixed-integer program. More precisely, we perform energy-efficient bicriteria lot-sizing and scheduling for one working week in which a deterministic demand must be satisfied. That is, only the quantities to be produced to meet the weekly demanded jobs differ between different working weeks. The current single-stage parallel machine environment consists of four machines with non-identical power coefficients, and the production speed of the machines is constant, i.e., cannot be throttled. In the following, we refer to this as process B.

Due to rising electricity prices and political pressure to achieve a more sustainable corporate structure, the company is now rethinking its processes:

- **Process B:** The current machinery is not changed.
- **Process A:** The machinery is similar to that of process B, i.e. the same power coefficients and the same maximum production output per hour, but the production speed is variable and each machine has a total of 10 different production speed levels.
- **Process A*:** The machines have different power coefficients and have a higher maximum production output per hour than the machines in processes A and B. The production speed is variable with less adjustable speed levels as in process A.

Table 5
Row-wise power ranking of the machines from best ($\widehat{=}1$) to worst ($\widehat{=}4$).

State	Machines m			
	$m=1$	$m=2$	$m=3$	$m=4$
Off	1	1	1	1
Ramp up	2	3	4	1
Standby	2	3	4	1
Production	1	3	2	4

Since production planning in the application example can be described by a bicriteria mixed-integer program, comparing and evaluating the different processes is equivalent to comparing different Pareto fronts. See Fig. 11 for an illustration of the applications' background.

The following assumptions are made when performing scheduling and lot-sizing:

- The planning horizon is one working week Mon–Fri 0 AM - 12 PM, divided into 120 h.
- All jobs are known at the beginning of the working week and the due dates are at the end of the working week.
- The electricity for production is purchased from the power market at variable hourly electricity prices (real-time pricing).
- The conflicting performance criteria are indirect emissions and electricity costs.
- The single-stage parallel machine environment consists of 4 machines whith non-identical electricity coefficients. This holds true in all processes A, A* and B.
- A power-down approach is considered, i.e., there are different machine states that satisfy the inequalities: off [kW] < standby [kW] <

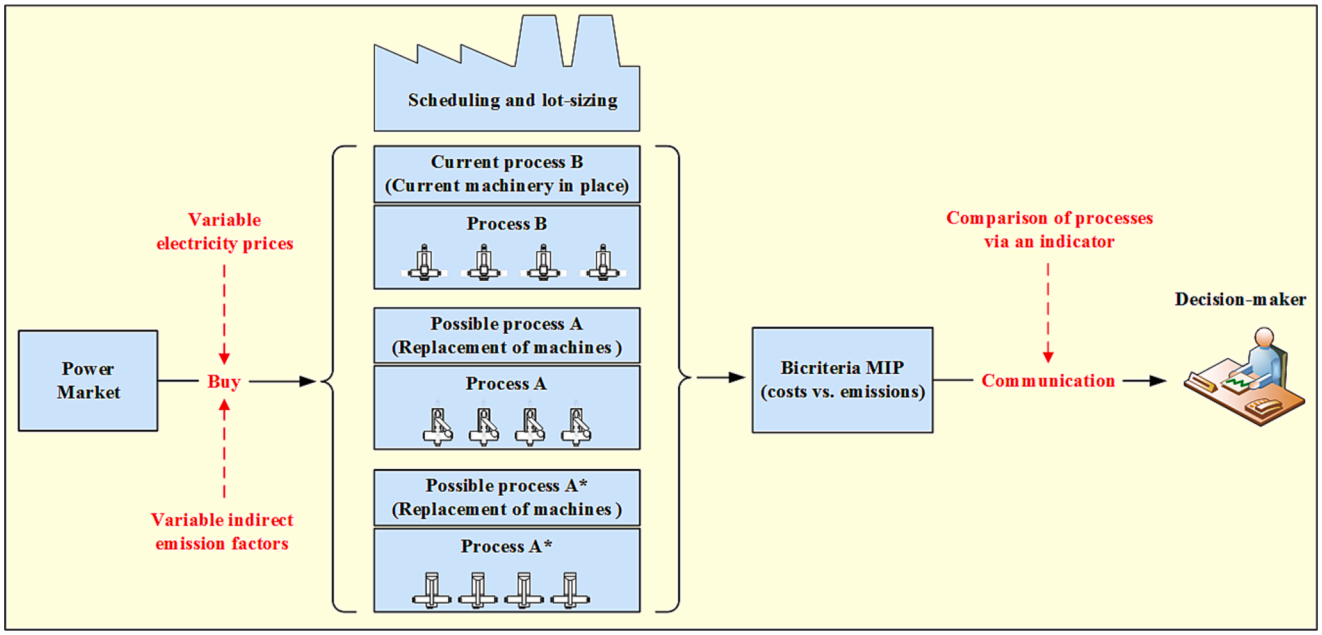

Fig. 11. Applications' background.

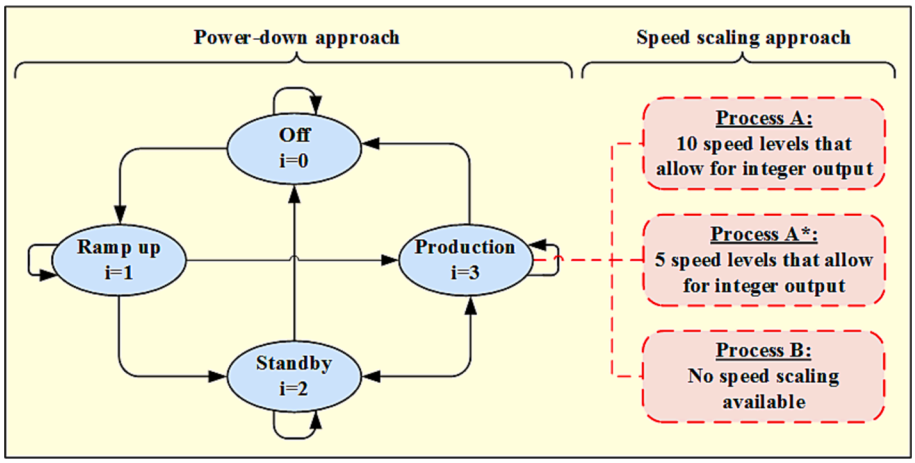

Fig. 12. Power-down approach and speed scaling approach.

ramp up [kW] < production [kW]. The power hierarchy, which applies to the three processes, is given in the following Table 5:

- A speed scaling approach is also taken into account: The machines of processes A and A* have discrete production speed levels that allow for an hourly integer output; The machines of process B have one uniform production speed level. See Fig. 12 for an illustration.
- The change in electricity consumption with variation of the production speed is calculated using the conversion formula found in Schulz et al. (2020).
- Preemption and lot-splitting are possible.
- A machine can process at most one job in one period, and the selected production speed cannot change in one period. The latter also applies to a selected machine state.
- For simplicity, warehousing, backlog and machine tooling are neglected.

The different processes include machines that differ in terms of the production speed: The machines of process B comprise constant production speed and those of processes A and A* encompasses throttleable production speed. To apply speed scaling, we require the following model-theoretic assumptions (Giglio et al., 2017; Schulz et al., 2020):

Table 6
Application setting.

	Process A	Process A*	Process B
Environment			
Machines	4 in parallel	4 in parallel	4 in parallel
Energy consumption	Heterogeneous	Heterogeneous	Heterogeneous
Process properties			
Preemption & lot splitting	Yes	Yes	Yes
Machine states (power-down)	Yes	Yes	Yes
Speed scaling	Yes (10 discrete levels)	Yes (5 discrete levels)	No
Production rate	Variable but discrete (max 10 per hour)	Variable but discrete (max 11 per hour)	Constant (10 per hour)
Planning horizon	1 week	1 week	1 week
Demand	Deterministic	Deterministic	Deterministic
Due date of jobs	End of week	End of week	End of week
Performance criteria			
Energy costs	Yes	Yes	Yes
Energy-related emissions	Yes	Yes	Yes

- There is a proportional relationship between the output of a machine and its production speed, i.e., throttling by 10% leads to an output reduction of 10%.
- Power consumption and production speed imply a non-proportional relationship.
- The production speed is constant between two consecutive discrete points in time.
- Only production speeds allowing an integer output per hour are feasible.

Each machine has a maximal production output per hour, i.e. the output at highest possible production speed $\nu_{maximal}$. To operationalize the aforementioned requirements, we simply subdivide the production rates of the maximal speed case. For example, let 10 quantities be the production output in one hour at speed $\nu_{maximal}$; then, in total, 10 different production speed levels $\nu \in \mathcal{N} = \{1, \ldots, 10\}$ with corresponding integer outputs $a_{\nu j}^{prod}$ can be realized, e.g., 100% of $\nu_{maximal} \rightsquigarrow a_{1j}^{prod} = 10$; 90% of $\nu_{maximal} \rightsquigarrow a_{2j}^{prod} = 9$, etc. To delineate the nonlinear relationship between power consumption and speed level in our lot-sizing and scheduling setting, we have adapted the transformation formula of Schulz et al. (2020), which was designed for pure scheduling problems:

$$\widehat{a}_{\nu m}^{elec\_I} = \left[1 + 0.6 \cdot \left(\frac{a_{1j}^{prod}}{a_{\nu j}^{prod}} - 1\right)^2 - 1.4 \cdot \left(\frac{a_{1j}^{prod}}{a_{\nu j}^{prod}} - 1\right)\right] \cdot a_{Im}^{elec} \cdot \frac{a_{\nu j}^{prod}}{a_{1j}^{prod}}, \tag{11}$$

where $\widehat{a}_{\nu m}^{elec\_I}$ is the resulting power consumption at speed level ν, a_{Im}^{elec} is the power consumption when producing at normal speed in production state I on machine m—in our case $I \widehat{=} i = 3$.

To briefly summarize this approach: The set of possible production speed levels is discrete, and the corresponding power consumption per hour of a machine at a given speed level can be calculated ex ante via (11); the resulting values then serve as input to the bicriterial mixed-integer program. An overview of the application setting is given in the following Table 6. For more details on the machines' parameters, see Appendix A.

3.3. Power market-related input data

The key input data driving the model are electricity prices and indirect emissions for the electricity mix purchased. They were determined for the German electricity market for 2020 on an hourly basis ($0-23h$) for a total of 4 working weeks (from Monday to Friday), one working week for each season (the data is taken from https://energy-charts.info and https://www.umweltbundesamt.de).

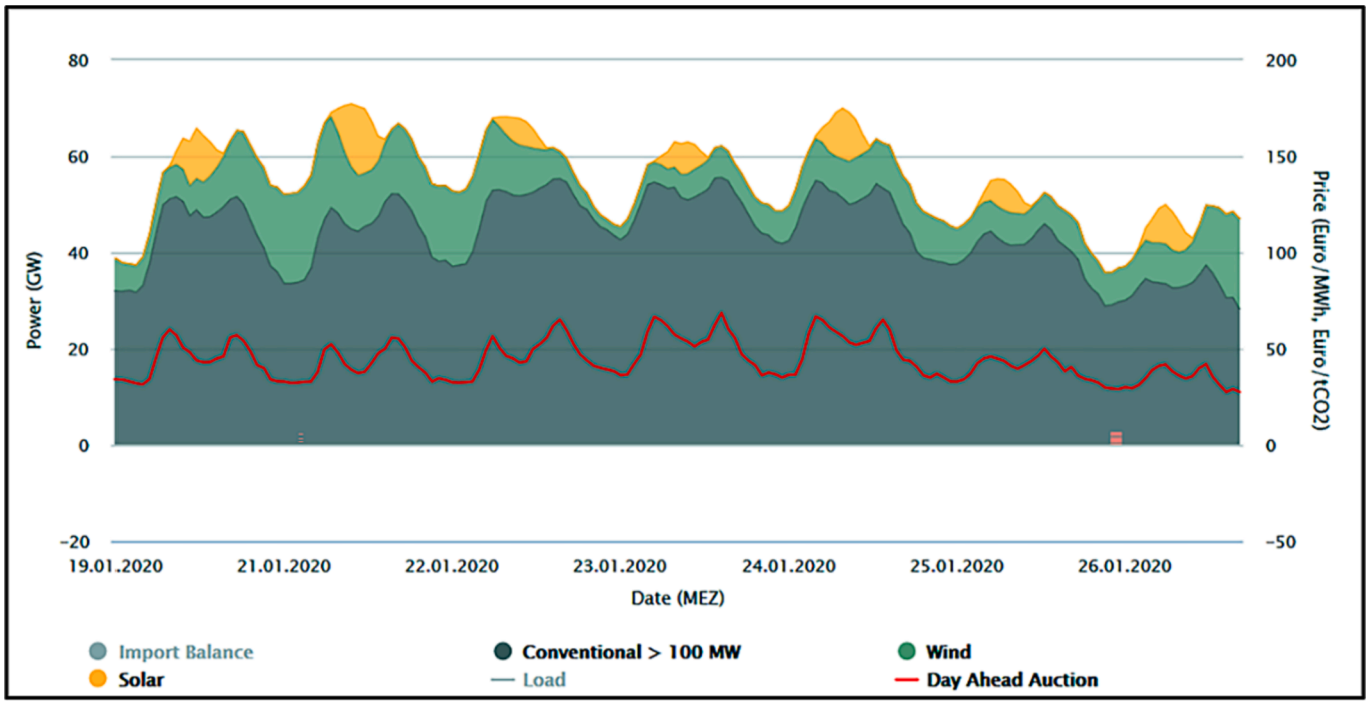

Fig. 13. Electricity production and spot prices in Germany in week 4 (2020).

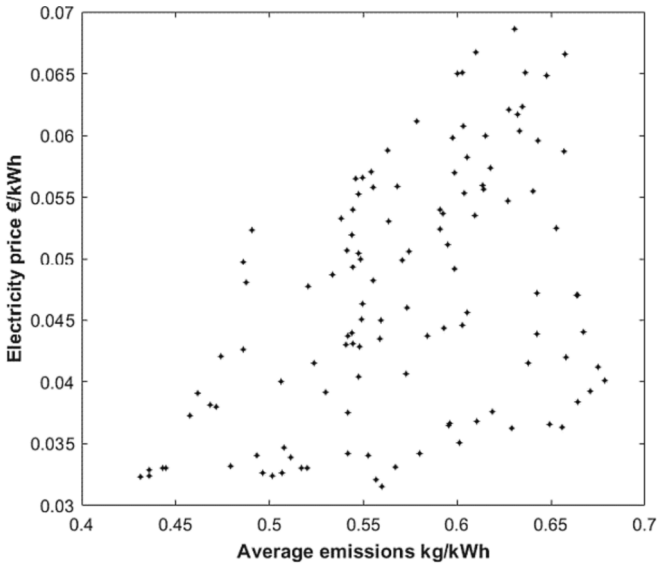

Fig. 14. Electricity prices and emissions.

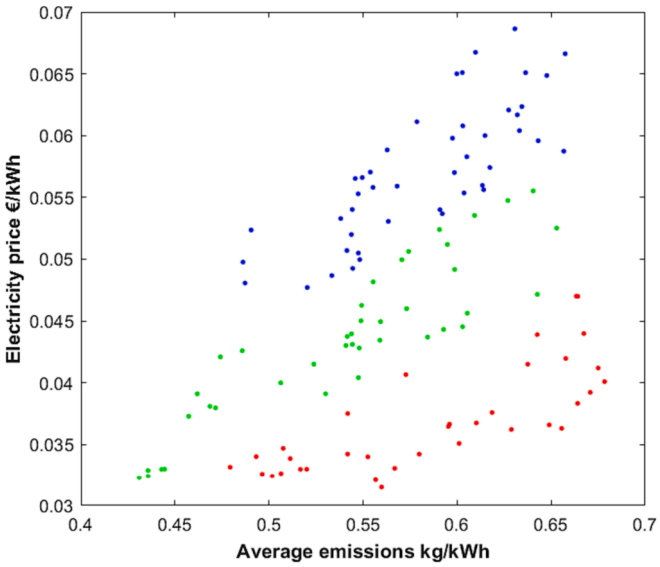

Fig. 15. K-means-based clustering.

Typical seasonal weather patterns have been used to obtain a more reliable picture (week 4, week 15, week 29, and week 41 of 2020), i.e., high wind and low solar in winter, mixed wind and solar in spring and fall, and low wind but high solar in summer. Fig. 13 illustrates an exemplary power generation profile and corresponding power prices for week 4 of 2020. In our study, we have used the hourly day-ahead prices from EPEX SPOT and calculated the hourly emission factors by applying the average values of the electricity source-specific emissions and their relative share in the hourly electricity mix.

To make the market-related conflict between electricity prices and emissions more transparent, we present electricity prices and average energy-related emissions for week 42,020 in Fig. 14. A visual inspection of Fig. 14 shows that the two features of the dataset—electricity prices and average emissions—do not appear to be collinear. To illustrate this, we perform unsupervised learning and want to partition the data points into three clusters according to three diagonal cuts as depicted in Fig. 15. Here, we want to obtain clusters where electricity prices are low, medium, and high relative to the corresponding average indirect emissions. Accordingly, we use K-means-based clustering with $K = 3$ and use cosine similarity as the similarity measure to obtain diagonal cuts (instead of the Euclidean similarity); see James et al. (2021).

Here, the abscissa shows the hourly average emissions [kg/kWh] and the ordinate the corresponding hourly electricity prices [€/kWh]. Obviously, electricity prices and energy-related average emissions are not perfectly positively correlated because the blue cluster contains data points with relatively low average emissions but relatively high electricity prices and vice versa in the case of the red one. The green cluster contains—more or less—non-conflicting points: the smaller the price,

Table 7
Indices, parameters, and variables.

Indices	
m	Machine $m \in \mathscr{M} = \{1, \ldots, M\}$
j	Job $j \in \mathscr{J} = \{1, \ldots, J\}$
i, h	States $i, h \in \mathscr{I} = \{0, \ldots, I\}$; 'off' ($i = 0$), 'ramp up' ($i = 1$), 'standby' ($i = 2$), 'production' ($i = 3$)
t	Period (a working hour) $t \in \mathscr{T} = \{0, \ldots, T\}$, $t = 0$ serves as initialization
ν	Production speed level $\nu \in \mathscr{N} = \{1, \ldots, N\}$
Parameters	
c_t^{elec}	Cost rate [€/kWh] of the electricity purchased in period t
e_t^{elec}	Carbon emission factor [kg/kWh] of the electricity mix purchased in period t
a_{ij}^{prod}	Hourly production rate of job j on each machine at speed level ν
d_j	Demand of job j
γ_{ih}^{tran}	Transition parameter from state i to h (1 if state transition is feasible, 0 otherwise)
a_{im}^{elec}	Electricity consumption of machine m in state i without $i = I$
$\widehat{a}_{\nu m}^{elec\_I}$	Electricity consumption of machine m in production state I at speed level ν
Decision variables	
$x_{jmt\nu}$	Equals 1 if job j will be processed on machine m in period t at speed level ν, otherwise 0
δ_{imt}^{state}	Equals 1 if machine m has state i in period t, Otherwise 0
$\widehat{\delta}_{mt\nu}^{state\_I}$	Equals 1 if machine m is in production state I at speed level ν in period t, otherwise 0
C	Equals the energy costs to be minimized
E	Equals the carbon emissions to be minimized
s_t^{buy}	Amount of electricity [kWh] to be purchased in period t

the smaller the emissions, and vice versa. The other 3 weeks show similar effects but are skipped to avoid overloading the paper.

3.4. Model setup

Table 7 provides the symbolics used in our mixed-integer optimization problem given by Eqs. (12)–(20). This program is suitable for modeling all three processes since only the coefficients and speed levels of the machines vary with respect to processes A, A* and B. In process B, for example, the machines have only one production speed level and thus, $\nu \in \mathscr{N} = \{1\}$.

$$min\ \mathrm{C} = \sum_{t=0}^{T} c_t^{elec} \cdot s_t^{buy} \tag{12}$$

$$min\ \mathrm{E} = \sum_{t=0}^{T} e_t^{elec} \cdot s_t^{buy} \tag{13}$$

$$\text{s.t.} \sum_{\nu=1}^{N} \sum_{t=0}^{T} \sum_{m=1}^{M} a_{vj}^{prod} \cdot x_{jmt\nu} = d_j \ \forall\ j \in \mathscr{J} \tag{14}$$

$$\sum_{i=0}^{I} \delta_{imt}^{state} = 1 \ \forall\ m \in \mathscr{M}, t \in \mathscr{T} \tag{15}$$

$$\widehat{\delta}_{mt\nu}^{state\_I} - \sum_{j=1}^{J} x_{jmt\nu} = 0 \ \forall\ t \in \mathscr{T}, m \in \mathscr{M}, \nu \in \mathscr{N} \tag{16}$$

$$\delta_{Imt}^{state} - \sum_{\nu=1}^{N} \widehat{\delta}_{mt\nu}^{state\_I} = 0 \ \forall\ t \in \mathscr{T}, m \in \mathscr{M} \tag{17}$$

$$\delta_{im,t-1}^{state} + \delta_{hmt}^{state} \leq 1 + \gamma_{ih}^{tran} \ \forall\ i, h \in \mathscr{I}, m \in \mathscr{M}, t \in \mathscr{T} \backslash \{0\} \tag{18}$$

$$\sum_{\nu=1}^{N} \sum_{m=1}^{M} \widehat{a}_{\nu m}^{elec\_I} \cdot \widehat{\delta}_{mt\nu}^{state\_I} + \sum_{\substack{i=0 \\ i \neq I}}^{I} \sum_{m=1}^{M} a_{im}^{elec} \cdot \delta_{imt}^{state} = s_t^{buy} \ \forall\ t \in \mathscr{T} \tag{19}$$

$$x_{jmt\nu}, \delta_{imt}^{state}, \widehat{\delta}_{mt\nu}^{state\_I} \in \{0, 1\}; s_t^{buy} \geq 0 \ \forall\ t \in \mathscr{T}, j \in \mathscr{J}, i \in \mathscr{I}, m \in \mathscr{M}, \nu \in \mathscr{N} \tag{20}$$

In this lot-sizing and scheduling problem, we minimize total energy costs C and total indirect emissions E, see (12) and (13). The objectives are determined by multiplying the electricity cost rate c_t^{elec} or emission factor e_t^{elec} for each period t by the energy consumption s_t^{buy} and aggregating accordingly.

Applying (14), we model an equality condition for meeting the demand d_j exactly concerning each job j, assuming there is no delay in the completion of orders—for simplification for this article. Eqs. (15) ensure that a machine has only one state in a period t and never becomes stateless. Eqs. (16) in combination with (17) control the production state in tandem with the speed level. That is, $\widehat{\delta}_{mt\nu}^{state\_I}$ equals 1 if any $x_{jmt\nu}$ equals 1 in (16). The latter is only the case when one job j is assigned to machine m at speed level ν in period t; otherwise, we have $\widehat{\delta}_{mt\nu}^{state\_I} = 0$. (17) couples the production mode $i = I$ ($i = 3$ in our case) of a machine m with one-speed level exclusively. Consequently, the sum over $\widehat{\delta}_{mt\nu}^{state\_I}$ is 1 or 0 otherwise.

In order to control the state transitions of a machine between two consecutive periods, we use (18). Here, a machine can either retain a state $\delta_{im,t-1}^{state} + \delta_{hmt}^{state} = 2$, with $h = i$ and $1 + \gamma_{ih}^{tran} = 2$, or can change it, with $h \neq i$. However, the latter case is only possible if the transition from state i to state h is feasible; if a transition is infeasible, γ_{ih}^{tran} is 0. Bear in mind that γ_{ih}^{tran} is a transition parameter given as input (see again Fig. 12). For further details, see Appendix A.

Eqs. (19) ensure that electricity consumption and purchased electricity s_t^{buy} are always in balance. Here, the electricity consumption for the production state (first doublesum) is treated separately from the other states (second doublesum) due to the finer-grained decomposition regarding the speed levels. (20) are typical binary and non-negativity conditions.

We initialize the model with the setting that all machines are in off mode in $t = 0$ and the machines should also be switched off at the end of a working week ($t = T$, here $T = 120$).

All calculations of Pareto fronts are conducted via GAMS using CPLEX. The calculations of the presented indicators for all Pareto fronts are conducted via MATLAB. Instances of the presented model are solved applying the ε-constraint method with a dynamically adaption of the ε stepsizes. The increase of the ε values is predominantly equidistant; however, when consecutive solutions differ, the algorithm checks this gap with a smaller stepsize. On the one hand, this reduces redundant computations that can occur if the preselected equidistant ε stepsizes are too small. On the other hand, a (discrete) Pareto front can be determined accurately this way. In addition, we apply a Pareto filter to weed out weakly efficient solutions. However, the anchor points of a Pareto front (i.e., the ideal point and nadir point), which determine the range of ε values to be varied, are obtained from the payoff table. More precisely, in the bicriteria case, a point that minimizes one objective leads to a tight upper bound for the other objective with respect to the Pareto front (if lexicographically optimized). For more details, see Chircop and Zammit-Mangion (2013) or Miettinen (1998).

4. Practicability of the new indicator

4.1. Scenario analysis: jobs with identical quantity requirements

Now we compute representations of Pareto fronts for the mixed-integer programs with respect to processes A, A*, and B. In this section, a scenario analysis is performed with 5 jobs and equal demand for each job in each scenario. In total, we generate 11 scenarios (S1, …, S11) in which the demand for each job increases uniformly up to approximately full capacity (based on the machinery in place) in the last scenario, see Table 8.

To demonstrate the practicality of the new indicator, corresponding indicator numbers for the Pareto front comparisons are calculated and compared with the classical indicators from Section 2.2. A justification

Table 8
Evenly distributed machine utilization.

	S1	S2	S3	S4	S5	S6	S7	S8	S9	S10	S11
Utilization	≈57%	≈61%	≈66%	≈70%	≈74%	≈78%	≈83%	≈87%	≈91%	≈95%	≈100%

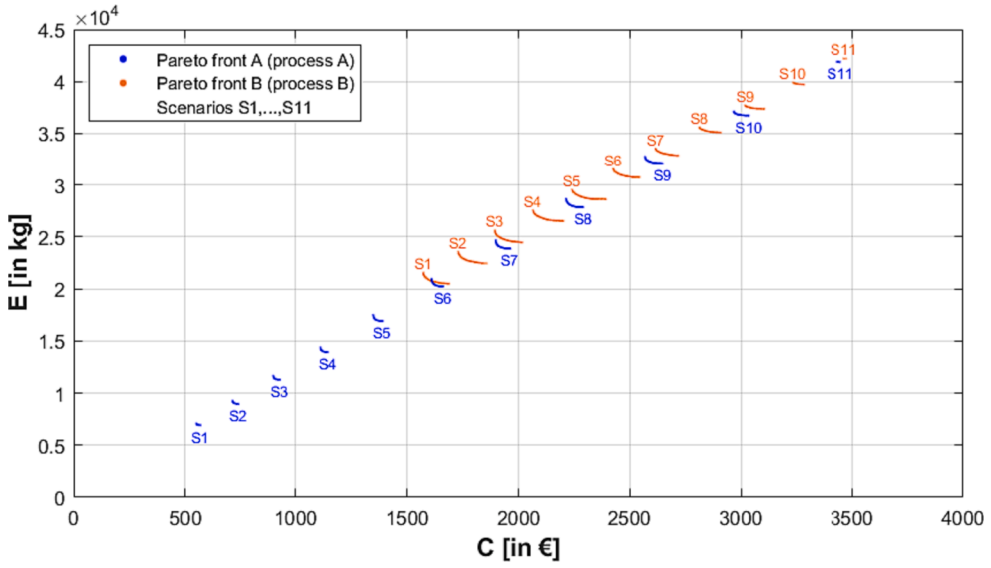

Fig. 16. Pareto fronts for all scenarios (processes A and B).

Table 9
Results for week 4 of 2020 (processes A and B).

	I_{GD}	I_{IGD}	I_{D1}	I_{D2}	I_{ϵ}	I_{HV}^{*}	I_{CoG}	I_{CoG}-triplet
S1	534.3574	426.8832	6759.4689	6791.191	2.9658	0.0059	0.6606	(0.6606, 0.6606, 0.6595)
S2	558.707	333.6682	6688.5549	6744.2083	2.5046	0.0066	0.5982	(0.5982, 0.5982, 0.596)
S3	521.3813	327.7379	6525.0019	6588.5607	2.1698	0.0069	0.5359	(0.5359, 0.5359, 0.5329)
S4	470.42	284.6783	6223.0565	6299.202	1.9057	0.0074	0.4719	(0.4719, 0.4719, 0.4685)
S5	466.5214	231.0403	5760.6626	5853.7847	1.6932	0.0082	0.4065	(0.4065, 0.4065, 0.4023)
S6	390.8624	190.0559	5136.6367	5253.2654	1.5206	0.0071	0.3401	(0.3401, 0.3401, 0.3352)
S7	413.5806	151.391	4365.647	4500.8771	1.3798	0.0063	0.2747	(0.2747, 0.2747, 0.2698)
S8	361.3616	126.8028	3500.6304	3630.1881	1.2696	0.0069	0.2086	(0.2086, 0.2086, 0.2049)
S9	425.0256	97.7548	2512.6275	2633.278	1.175	0.0076	0.1433	(0.1433, 0.1433, 0.1414)
S10	273.9165	69.8954	1417.6945	1492.6292	1.0896	0.0072	0.0771	(0.0771, 0.0771, 0.077)
S11	148.2886	29.7958	153.5602	163.5763	1.009	0.0089	0.0081	(0.0081, 0.0081, 0.0083)
∅	414.9475	206.3366	4458.5037	4540.9783	1.6984	0.0072	0.3386	(0.3386, 0.3386, 0.336)

for identical jobs can be found in Pinedo (2016). A scenario analysis with non-identical order quantities will be performed in the next section.

Comparison of process A and process B

Fig. 16 shows the results for the winter season, i.e., week 4 of 2020.

A visual inspection of Fig. 16 reveals that the short-term production plans with respect to process B result in generally higher energy costs and indirect emissions than those with respect to process A. The differences become smaller the higher the capacity utilization. In the latter scenario, the advantage of process A over process B almost disappears. Therefore, a process change from B to A is only recommended if there is capacity flexibility to meet the requested quantities. In the latter scenarios, however, this is rarely the case, as the machines must produce at maximum speed in almost every time slot to meet demand.

However, all graphs, methods, and respective results or observations—that also fit the other weeks—are easily accessible for professionals; this may not always apply to a decision-maker. In addition, here, visual inspection provides only approximate information. Condensing this information into a quantitative statement is a more accurate means of aiding decision making. Therefore, Table 9 summarizes the results regarding all indicators presented, applying $w_1 = 0.5$, $w_2 = 0.5$. As reference value in I_{HV}^{*}, we use the nadir point of front B (depending on the scenario) plus the vector $(0.001, 0.001)^{\top}$.

Table 10
Results for four weeks of 2020: Component-wise indicator I_{CoG}^{comp}.

	I_{CoG}^{comp}										
	S1	S2	S3	S4	S5	S6	S7	S8	S9	S10	S11
	$\begin{pmatrix}0.6557\\0.6655\end{pmatrix}$	$\begin{pmatrix}0.5944\\0.602\end{pmatrix}$	$\begin{pmatrix}0.5316\\0.5402\end{pmatrix}$	$\begin{pmatrix}0.4671\\0.4766\end{pmatrix}$	$\begin{pmatrix}0.4035\\0.4094\end{pmatrix}$	$\begin{pmatrix}0.3392\\0.341\end{pmatrix}$	$\begin{pmatrix}0.2787\\0.2707\end{pmatrix}$	$\begin{pmatrix}0.2134\\0.2039\end{pmatrix}$	$\begin{pmatrix}0.1492\\0.1374\end{pmatrix}$	$\begin{pmatrix}0.0808\\0.0733\end{pmatrix}$	$\begin{pmatrix}0.0087\\0.0075\end{pmatrix}$

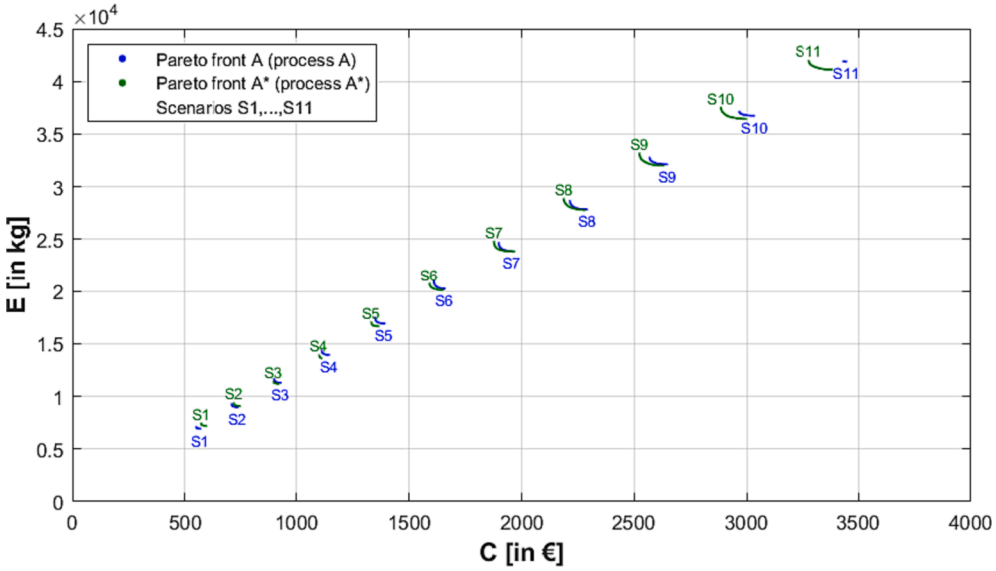

Fig. 17. Pareto fronts for all scenarios (processes A and A*).

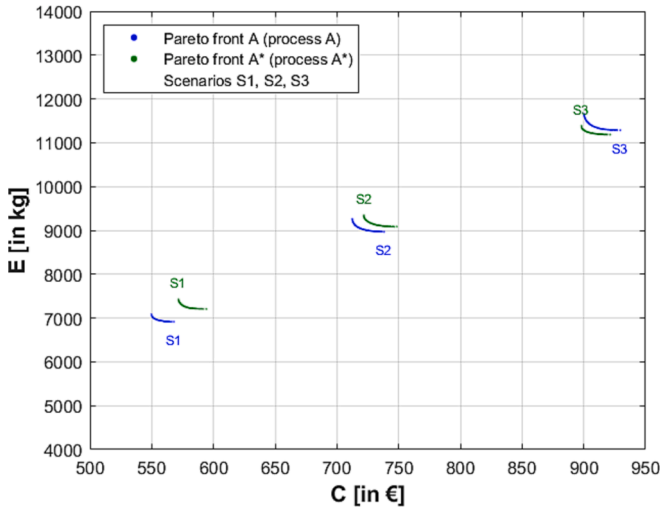

Fig. 18. Pareto fronts for scenario S1-S3.

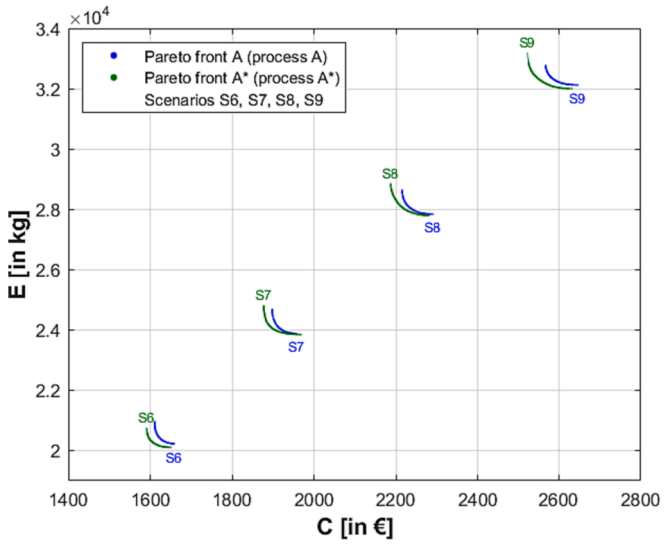

Fig. 19. Pareto fronts for scenario S6-S9.

From this Table 9, one can learn that the indicator values I_{IGD}, I_{D1} and I_{D2} decrease monotonically but are associated with high absolute values compared to the other indicators in each scenario. Neither I_{GD} nor I_{HV} shows a monotonic behavior, see, e.g., **S6**–**S10**. The values of I_ϵ also decrease monotonically but on a lower absolute level than I_{IGD}, I_{D1} and I_{D2}. However, all these indicators do not allow for a more precise objective-related statement, while this is the case with I_{CoG}. It shows a monotonic behavior and allows concrete statements such as: "in scenario **S1**, energy costs, and indirect emissions can be improved by approx. 66.1% on average when changing processes from B to A."

In the last column of Table 9, we give the numbers of the I_{CoG}-triplet, that is, the value of I_{CoG} with respect to an unpruned front (first component) and a minimally and Euclidean-pruned front, respectively (second and third components). Since all components are positive, we can infer that A▷B, i.e., front A is better than front B in every scenario. However, the interpretation is then based on the smallest positive component (see again Table 4).

In all scenarios, we calculated the values of I_{CoG} using the weights $w_1 = 0.5, w_2 = 0.5$. However, we can use I_{CoG}^{comp} for the unweighted version of I_{CoG}, which gives us the average percentage deviation for each objective, see Table 10.

Overall, the process A is superior to process B. More specifically, based on the I_{CoG}, the energy costs and indirect emissions can be improved on average by about 34.86% (see the last row of Table 9) when swapping from process B to process A. Such meaningful statements cannot be derived from the other indicators presented.

Comparison of Process A and Process A*

So far, we have observed that process A is preferred over process B. Now we compare process A to A* accordingly.

Fig. 17 shows the Pareto fronts with respect to processes A and A* for all scenarios. Figs. 18 and 19 highlight the Pareto fronts for selected scenarios. As observed, the Pareto fronts' order changes throughout the scenarios. More precisely, Pareto front A is preferred over A* in scenarios 1 and 2, i.e., at about 57% and 61% capacity utilization. Pareto front A* is preferred over Pareto front A in the remaining scenarios. In Fig. 19, one Pareto front does not weakly totally dominate the other Pareto front (see Definition 6), as was the case in Fig. 16 when comparing processes A and B. As a result, the shortcomings of I_{CoG} may come into play, but can be remedied by applying the pruning strategies

Table 11
Results for week 4 of 2020 (processes A and A*).

	I_{GD}	I_{IGD}	I_{D1}	I_{D2}	I_ϵ	$I_{HV}^{z^*}$	I_{CoG}-triplet
S1	13.9635	15.7003	114.2463	146.5043	1.0426	0.9613	(0.0408, 0.0408, 0.0376)
S2	1.3142	3.4377	22.5156	58.2164	1.013	0.984	(0.0118, 0.0118, 0.0105)
S3	4.3252	5.8455	0	0	0.9977	1.0091	(−0.0093, −0.0093, −0.0081)
S4	24.3827	11.5808	0	0	0.99	1.0347	(−0.0215, −0.0215, −0.0162)
S5	12.6663	8.5396	0	0	0.9881	1.0368	(−0.0173, −0.0173, −0.0138)
S6	2.9108	2.9976	0	0	0.9941	1.0311	(−0.0096, −0.0096, −0.0088)
S7	0.9016	0.7906	0	0	0.999	1.0283	(0.0012, −0.0038, −0.0047)
S8	1.0658	0.8869	0	0	0.9984	1.0454	(−0.004, −0.0041, −0.0044)
S9	3.514	1.6454	0	0	0.9965	1.1029	(−0.0064, −0.0069, −0.0076)
S10	6.6709	4.2295	0	0	0.9915	1.3624	(−0.0123, −0.0124, −0.0142)
S11	20.9549	25.1575	0	0	0.9822	13.8594	(−0.0246, −0.0247, −0.024)
∅	8.4245	7.3465	12.4329	18.6110	0.9994	2.2232	(−0.0047, −0.0052, −0.0049)

Table 12
Results for week 4 of 2020 (processes A* and B).

	S1	S2	S3	S4	S5	S6	S7	S8	S9	S10	S11	∅
I_{CoG}	0.646	0.593	0.5398	0.483	0.4162	0.3458	0.2766	0.2113	0.1481	0.088	0.0318	0.3436

developed in Section 2.4 and using the I_{CoG}-triplet.

Overall, the visual inspection could lead to the conclusion that process A* is the process of choice in the transformation of the company structure because this process is superior from a capacity utilization of about 61% than process A. However, we want to compress this result in a quantitive statement for communication purposes. Table 11 depicts the corresponding numbers of the indicators. Again, applying $w_1 = 0.5$, $w_2 = 0.5$ and as reference value in $I_{HV}^{z^*}$, we use a vector that is worse than each of the nadir points of front A and A* in a scenario.

Here, we apply Pareto front A as the first input and front A* as the second input to compute the respective binary indicators. However, the order of the Pareto fronts changes from scenario S3 onwards. The indicators I_{GD} and I_{IGD} fail to identify this change. The indicators I_{D1}, I_{D2}, I_ϵ and $I_{HV}^{z^*}$ illustrate the change in the order, but their values remain questionable in terms of concrete economic and/or ecological implications. Even worse, for the indicators I_{GD} and I_{IGD} as well as I_{D1}, I_{D2}, the order of the Pareto fronts has to be determined theoretically a priori, and the calculations have to be adjusted on the basis of the determined structure. When a large number of scenarios is calculated, visual identification is very time-consuming, if possible at all. Therefore, the order of the fronts has to be determined algorithmically.

However, Table 11 reveals the superiority of the novel indicator regarding communication purposes. First, the I_{CoG}-triplet shows the change in the order of the Pareto fronts (see again Table 4). Misclassifications like in scenario S7 are detected and removed by the developed pruning strategies. Overall, taking the average of all scenarios, the interpretation is as follows: On average, the relative performance with respect to the performance measures under consideration deteriorates by about 0.5% when swapping from process A* to process A.

For completeness, Table 12 shows the I_{CoG} values for the comparison between Process A* and Process B.

4.2. Scenario analysis: jobs with non-identical quantity requirements

We now relax the requirement that the jobs have identical order requirements. More specifically, the integer number of orders is generated uniformly at random, ranging from 5 to 8 orders. The demanded quantities of a job are also randomly generated, and the total demanded quantities range from about 65% to 85% of the capacity utilization of the existing machines (i.e., with respect to process B). Consequently, a total of 30 different settings is generated. Tables 13 and 14 show an excerpt of the results (for the complete tables, see Tables B1 and B2 in Appendix B). Here, since fronts A or A* weakly totally dominate B, the values of I_{CoG} are sufficient instead of the triplet.

While the already established indicators show only limited applicability for communication purposes, the I_{CoG} allows an overall statement over the course of the scenarios. More precisely, when changing from process B to process A, the performance objectives improve by an average of about 38.64%. However, the average improvement potential regarding the performance objectives is by about 0.6% larger when changing from process B to process A*.

As a *se*condary result, Table 15 shows the average computation times for calculating the indicators across all scenarios. It can be seen that the proposed indicator I_{CoG} requires less computation time (and thus less effort) than the other indicators. However, the computational effort required to calculate the indicators is negligible for the present study, but could become relevant in more complex problems (e.g., in cases with more than two objectives).

Next, we will show that I_{CoG} can be approximated a priori to reduce the computational cost of solving instances of the mixed-integer program given by (12)–(20).

Table 13
Results for week 4 of 2020 (processes A and B).

	I_{GD}	I_{IGD}	I_{D1}	I_{D2}	I_ϵ	$I_{HV}^{z^*}$	I_{CoG}
S1 (≈77%)	1287.9949	576.2229	5321.1144	5447.1953	1.5686	0.0078	0.3615
S2 (≈77%)	1200.6199	824.7776	5370.2364	5475.7738	1.5768	0.0080	0.3648
S3 (≈69%)	1256.1310	990.3451	6259.0106	6350.6096	1.9415	0.0073	0.4829
…	…	…	…	…	…	…	…
S28 (≈71%)	1341.6428	1356.1072	6040.6451	6160.3926	1.8258	0.0072	0.4495
S29 (≈80%)	1146.1918	568.3365	4834.3542	5003.5188	1.4681	0.0070	0.3180
S30 (≈79%)	1091.2970	812.1745	5018.9691	5148.9065	1.4977	0.0058	0.3307
∅	1264.3897	871.1103	5431.7627	5558.7466	1.6673	0.0069	0.3864

Table 14
Results for week 4 of 2020 (processes A* and B).

	I_{GD}	I_{IGD}	I_{D1}	I_{D2}	I_{ϵ}	I^{-}_{HV}	I_{CoG}
S1 (≈77%)	1321.0200	2371.4556	5410.7762	5531.6068	1.5845	0.0076	0.3672
S2 (≈77%)	1228.0492	10,609.0477	5281.0532	5281.0532	1.5794	0.0081	0.3684
S3 (≈69%)	1296.6797	1427.8247	6440.9774	6506.8217	1.9874	0.0071	0.4929
…	…	…	…	…	…	…	…
S28 (≈71%)	1393.6498	2319.6247	6221.9583	6337.7514	1.8705	0.0069	0.4604
S29 (≈80%)	1160.8658	1809.1696	4933.1835	5041.9389	1.4761	0.0068	0.3214
S30 (≈79%)	1116.7594	4102.5809	5002.5003	5197.6869	1.5049	0.0056	0.3334
∅	1294.1766	2833.7128	5516.5407	5633.1416	1.6890	0.0067	0.3924

Table 15
Mean computation times of the indicators over S1-S30.

	I_{GD}	I_{IGD}	I_{D1}	I_{D2}	I_{ϵ}	I^{-}_{HV}	I_{CoG}
∅-CPU in sec. (A and B)	0.0294	0.0781	0.0777	0.0779	0.0779	0.0843	0.0002
∅-CPU in sec. (A* and B)	0.0293	0.0195	0.0202	0.0199	0.0198	0.0857	0.0002

4.3. Approximation of the new indicator I_{CoG}

Due to the generally high computational complexity of a mixed-integer problem, determining an exact Pareto front is often very time-consuming, especially in bicriteria production planning (Seeanner & Meyr, 2013; Meyr, 2002; Brüggemann & Jahnke, 2000). In our analysis, for example, for processes A and B, the smallest capacity utilization scenarios took a few hours to obtain the Pareto fronts. To approximate the new indicator I_{CoG}, we make use of a principle we call the *principle of fixed data*; the following proposition provides it:

Proposition 2. (Principle of fixed data). *Suppose the electricity prices and emission factors are constant,* i.e. $c^{elec}_t = c^{fix}, e^{elec}_t = e^{fix} \forall t \in \mathcal{T}$ *and positive* $c^{fix}, e^{fix} \in \mathbb{R}_{>0}$. *Then,* I_{CoG} *based on (12)–(20) is independent of* c^{fix}, e^{fix}.

Proof:

Let $c^{fix}, e^{fix} > 0$. An optimal solution exists since the feasible set given by (14)–(20) is compact. For (12) and (13), we then get

$$\mathrm{C} = \sum_{t=0}^{T} c^{fix} \cdot s^{buy}_t = c^{fix} \sum_{t=0}^{T} s^{buy}_t; \mathrm{E} = \sum_{t=0}^{T} e^{fix} \cdot s^{buy}_t = e^{fix} \sum_{t=0}^{T} s^{buy}_t.$$

It follows that minimizing C and E leads to minimizing $\sum_{t=0}^{T} s^{buy}_t$, since s^{buy}_t is independent of c^{fix} and e^{fix} in (14)–(20) $\forall t$, leading to a singleton Pareto front.

Now, let $s^*_{\mathrm{A}} > 0$ and $s^*_{\mathrm{B}} > 0$ be the minmal aggregated energy consumption for Process A and Process B—wrt. (14)–(20)—for any arbitrary scenario. The indicator I_{CoG} then reads:

$$I_{CoG}\left(s^*_{\mathrm{A}} \cdot \begin{pmatrix} c^{fix} \\ e^{fix} \end{pmatrix}, s^*_{\mathrm{B}} \cdot \begin{pmatrix} c^{fix} \\ e^{fix} \end{pmatrix}\right) = 1 - \left(w_1 \cdot \frac{s^*_{\mathrm{A}} \cdot c^{fix}}{s^*_{\mathrm{B}} \cdot c^{fix}} + w_2 \cdot \frac{s^*_{\mathrm{A}} \cdot e^{fix}}{s^*_{\mathrm{B}} \cdot e^{fix}}\right)$$
$$= 1 - \underbrace{(w_1 + w_2)}_{=1} \cdot \frac{s^*_{\mathrm{A}}}{s^*_{\mathrm{B}}} = 1 - \frac{s^*_{\mathrm{A}}}{s^*_{\mathrm{B}}}.$$

Here, assuming $s^*_{\mathrm{B}} > 0$ and $s^*_{\mathrm{A}} > 0$ precludes non-production or zero-demand scenarios. As a consequence, the indicator I_{CoG} is independent of c^{fix}, e^{fix}. □

Due to the principle of fixed data, we can approximate the indicator I_{CoG} solving only two instances of the model given by (12)–(20), one for each process B and A (or A*), respectively. For week 4 of 2020, the approximation results are presented in Table 16.

Here, the maximal absolute deviation $|\Delta|$ is 0.0128 in **S3**, i.e., it differs by about 1.28% from the exact value. Obviously, this is a fairly good method for determining the overall—economic and ecological—advantage of production process changes.

As proven above, the approximation is independent of the electricity prices and emissions; however, the quality of the approximation also depends on the dispersion of the input data of course. In Table 17, the empirical standard deviations for the input data are determined. We see that if the empirical standard deviation increases, then the maximal absolute approximation error also tends to increase; the highest approximation error can be found in week 15 of 2020.

Overall, we have uncovered the potential of the new indicator and its very good approximation results. The next section concludes this article.

Table 17
Dispersion aspects.

	week 4	week 15	week 29	week 41
SD of electricity prices	0.01	0.0087	0.0076	0.0112
SD of emission factors	0.0605	0.1063	0.0807	0.0664
maximal $\|\Delta\|$	0.0128	0.0253	0.0126	0.0188

5. Conclusions

In this paper, we have developed an indicator based on the Centers of Gravity (CoG) of different Pareto fronts—derived from bicriteria production planning problems. The novel indicator shows great potential when, for example, analyzing production process transformations due to its efficiency change-related statement, which can be directly applied to the individual criteria. Additionally, the indicator still provides interpretable information when it comes to higher dimensions, i.e., more than two objective functions. This might be an essential indicator feature, especially when the Pareto fronts cannot be adequately visualized. From a computational point of view, the indicator is less expensive than the most common indicators in literature. The superiority of our indicator is demonstrated via a sustainable bicriteria lot-sizing and

Table 16
Approximation results for week 4 of 2020 – identical order requirements.

	S1	S2	S3	S4	S5	S6	S7	S8	S9	S10	S11
I^{Approx}_{CoG}	0.6694	0.6098	0.5487	0.4823	0.416	0.3482	0.2792	0.2094	0.142	0.0748	0.0068
I_{CoG}	0.6606	0.5982	0.5359	0.4719	0.4065	0.3401	0.2747	0.2086	0.1433	0.0771	0.0081
$\|\Delta\|$	0.0088	0.0116	0.0128	0.0104	0.0095	0.0081	0.0045	0.0008	0.0013	0.0023	0.0013

scheduling problem, performing a scenario analysis for a metal-working company, where time-dependent energy costs and indirect carbon dioxide emissions are minimized simultaneously. In this context, we have developed an a priori approximation approach which leads to promising results. However, the CoG-based indicator can be distorted if, for example, the diameters or spreading of Pareto fronts are relatively large. For such cases, we develop pruning concepts and algorithms to retain the indicator's properties. Several aspects could be useful for further research. First, can we generalize the indicator to compare Pareto fronts that are unorderable from a dominance analysis-based perspective? Second, how do different metrics affect the pruning of a Pareto front and thus the CoG-based indicator? Third, production planning under more than two performance criteria or in interaction with metaheuristic procedures can be analyzed. These aspects could be rewarding topics for future research.

CRediT authorship contribution statement

Markus Hilbert: Conceptualization, Methodology, Formal analysis, Writing – original draft, Validation, Visualization. **Andreas Dellnitz:** Methodology, Formal analysis, Writing – original draft, Validation, Visualization. **Andreas Kleine:** Methodology, Writing – review & editing, Validation, Visualization. **Madjid Tavana:** Formal analysis, Writing – review & editing, Validation, Visualization.

Declaration of Competing Interest

The above authors declare that they have no known competing financial interests or personal relationships that could have appeared to influence the work reported in this paper.

Data availability

No data was used for the research described in the article.

Appendix A. Supplementary data

Supplementary data to this article can be found online at https://doi.org/10.1016/j.cie.2023.109618.

References

Alexopoulos, I., Kounetas, K., & Tzelepis, D. (2018). Environmental and financial performance. Is there a win-win or a win-loss situation? Evidence from the greek manufacturing. *Journal of Cleaner Production, 197*(1), 1275–1283. https://doi.org/10.1016/j.jclepro.2018.06.302

Anghinolfi, D., Paolucci, M., & Ronco, R. (2021). A bi-objiective heuristic aaproach for green identical parallel machine scheduling. *European Journal of Operational Research, 289*(2), 416–434. https://doi.org/10.1016/j.ejor.2020.07.020

Audet, C., Bigeon, J., Cartier, D., Le Digabel, S., & Salomon, L. (2021). Performance indicators in multiobjective optimization. *European Journal of Operational Research, 292*, 397–422. https://doi.org/10.1016/j.ejor.2020.11.016

Bänsch, K., Busse, J., Meisel, F., Rieck, J., Scholz, S., Volling, T., & Wichmann, M. (2021). Energy-aware decision support models in production environments: A systematic literature review. *Computers & Industrial Engineering, 159*, 107456. https://doi.org/10.1016/j.cie.2021.107456

Biel, K., & Glock, C. (2016). Systematic literature review of decision support models for energy-efficient production planning. *Computers & Industrial Engineering, 101*, 243–259. https://doi.org/10.1016/j.cie.2016.08.021

Brüggemann, W., & Jahnke, H. (2000). The discrete lot-sizing and scheduling problem: Complexity and modification for batch availability. *European Journal of Operational Research, 511–528*. https://doi.org/10.1016/S0377-2217(99)00190-3

Chen, T., Cheng, C., & Chou, Y. (2020). Multi-objective genetic algorithm for energy-efficient hybrid flow shop scheduling with lot streaming. *Annals of Operations Research, 290*, 813–836. https://doi.org/10.1007/s10479-018-2969-x

Chircop, K., & Zammit-Mangion, D. (2013). On epsilon-constraint based methods for the generation of pareto frontiers. *Journal of Mechanics Engineering and Automation, 3*(5), 279–289.

Coello, C., & Cortés, N. (2005). Solving multi-objective optimization problems using an artificial immune system. *Genetic Programming and Evolvable Machines, 6*, 163–190. https://doi.org/10.1007/s10710-005-6164-x

Collette, Y., & Siarry, P. (2004). *Multi-objective optimization* (2 ed.). Springer. https://doi.org/10.1007/978-3-662-08883-8

Copil, K., Wörbelauer, M., Meyr, H., & Tempelmeier, H. (2017). Simultaneous lotsizing and scheduling problems: A classification and review of models. *OR Spectrum, 39*, 1–64. https://doi.org/10.1007/s00291-015-0429-4

Cui, W., & Lu, B. (2021). Energy-aware operations management for flow shops under TOU electricity tariff. *Computers & Industrial Engineering, 151*, 106942. https://doi.org/10.1016/j.cie.2020.106942

Czyżżak, P., & Jaszkiewicz, A. (1998). Pareto simulated annealing - a metaheuristic technique for multiple objective combinatorial optimization. *Journal of Multi-Criteria Decision Analysis, 7*(1), 34–47. https://doi.org/10.1002/(SICI)1099-1360(199801)7:1<34::AID-MCDA161>3.0.CO;2-6

Deb, K., & Jain, S. (2004). Evaluating evolutionary multi-objective optimization algorithms using running performance metrics. In K. Tan, M. Lim, X. Yao, & L. Wang (Eds.), *Recent advances in simulated evolution and learning* (pp. 307–326). World Scientific. https://doi.org/10.1142/9789812561794_0017.

Dellnitz, A., Braschczok, D., Ostmeyer, J., Hilbert, M., & Kleine, A. (2020). Energy costs vs. carbon dioxide emissions in short-term production planning: A business case study. *Journal of Business Economics, 90*, 1383–1407.

Ding, J., Schulz, S., Shen, L., Buscher, U., & Lü, Z. (2021). Energy aware scheduling in flexible flow shops with hybrid particle swarm optimization. *Computers & Operations Research, 125*(105088). https://doi.org/10.1016/j.cor.2020.105088

Ding, J., Song, S., & Wu, C. (2016). Carbon-efficient scheduling of flow shops by multi-objective optimization. *Journal of Cleaner Production, 197*(1), 1275–1283. https://doi.org/10.1016/j.ejor.2015.05.019

Dong, C., Shen, B., Chow, P., Yang, L., & Ng, C. (2016). Sustainability investment under cap-and-trade regulation. *Annals of Operations Research, 240*, 509–531. https://doi.org/10.1007/s10479-013-1514-1

Dong, J., & Ye, C. (2022). Green scheduling of distributed two-stage reentrant hybrid flow shop considering distributed energy resources and energy storage system. *Computers & Industrial Engineering, 169, 108146*. https://doi.org/10.1016/j.cie.2022.108146

Dyer, M., & Frieze, A. (1988). On the complexity of computing the volume of a polyhedron. *SIAM Journal on Computing, 17*, 967–974. https://doi.org/10.1137/0217060

Ehrgott, M. (2005). *Multicriteria optimization* (2 ed.). Springer. https://doi.org/10.1007/3-540-27659-9

EU-COM – European Commission. (2020). *A new industrial stratey for Europe*. Communication from the Commission. https://eur-lex.europa.eu/legal-content/EN/TXT/?qid=1593086905382&uri=CELEX%3A52020DC0102.

Gahm, C., Denz, F., Dirr, M., & Tuma, A. (2016). Energy-efficient scheduling in manufacturing companies: A review and research framework. *European Journal of Operational Research, 248*(3), 744–757. https://doi.org/10.1016/j.ejor.2015.07.017

Giglio, D., Paolucci, M., & Roshani, A. (2017). Integrated lot sizing and energy-efficient job shop scheduling problem in manufacturing/remanufacturing systems. *Journal of Cleaner Production, 148*, 624–641. https://doi.org/10.1016/j.jclepro.2017.01.166

Gong, X., & Zhou, S. (2013). Optimal production planning with emissions trading. *Operations Research, 61*(4), 908–924. https://doi.org/10.1287/opre.2013.1189

Gu, W., Li, Z., Dai, M., & Yuan, M. (2021). An energy-efficient multi-objective permutation flow shop scheduling problem using an improved hybrid cuckoo search algorithm. *Advances in Me-chanical Engineering, 13*, 1–15. https://doi.org/10.1177/16878140211023603

Ho, M., Hnaien, F., & Dugardin, F. (2022). Exact method to optimize the total electricity cost in two-machine permutation flow shop scheduling problem under time-of-use tariff. *Computers & Operations Research, 144*(105788). https://doi.org/10.1016/j.cor.2022.105788

Hogarth, R., & Soyer, E. (2015). Providing information for decision making: Contrasting description and simulation. *Journal of Applied Research in Memory and Cognition, 4*(3), 221–228. https://doi.org/10.1016/j.jarmac.2014.01.005

Holland, S., & Mansur, E. (2008). Is real-time pricing green? The environmental impacts of electricity demand variance. *The Review of Economics and Statistics, 90*(3), 550–561. https://doi.org/10.1162/rest.90.3.550

Jaehn, F. (2016). Sustainable operations. *European Journal of Operational Research, 253*, 243–264. https://doi.org/10.1016/j.ejor.2016.02.046

James, G., Witten, D., Hastie, T., & Tibshirani, R. (2021). *An intorduction to statistical learning*. Springer. https://doi.org/10.1007/978-1-4614-7138-7

Kallrath, J. (2021). *Business optimization using mathematical programming*. Springer. https://doi.org/10.1007/978-3-030-73237-0

Knowles, J., & Come, D. (2002). On metrics comparing nondominated sets. In *Proceedings of the 2002 congress on evolutionary computation (CEC)* (pp. 711–716). https://doi.org/10.1109/CEC.2002.1007013

Lewis, A., Mostaghim, S., & Randall, M. (2008). Evolutionary population dynamics and multi-objective optimisation problems. *Multi-Objective Optimization in Computational Intelligence: Theory and Practice*. https://doi.org/10.4018/978-1-59904-498-9.ch007

Li, Y., Yang, Z., Wang, L., Tang, H., Sun, L., & Guo, S. (2022). A hybrid imperialist competitive algorithm for energy-efficient flexible job shop scheduling problem with variable-size sublots. *Computers & Industrial Engineering, 172*, 108641. https://doi.org/10.1016/j.cie.2022.108641

Liang, J., Wang, Y., Zhang, Z., & Sun, Y. (2019). Energy efficient production planning and scheduling problem with processing technology selection. *Computers & Industrial Engineering, 132*, 260–270. https://doi.org/10.1016/j.cie.2019.04.042

Liu, C., & Huang, D. (2014). Reduction of power consumption and carbon footprints by applying multi-objective optimisation via genetic algorithms. *International Journal of Production Research, 52*, 337–352. https://doi.org/10.1080/00207543.2013.825740

Luo, H., Du, B., Huang, G., Chen, H., & Li, X. (2013). Hybrid flow shop scheduling considering machine electricity consumption cost. *International Journal of Production Economics, 146*, 423–439. https://doi.org/10.1016/j.ijpe.2013.01.028

Maecker, S., & Shen, L. (2020). Solving parallel machine problems with delivery times and tardiness objectives. *Annals of Operations Research, 285*, 315–334. https://doi.org/10.1007/s10479-019-03267-2

Mansouri, A., Aktas, E., & Besikci, I. (2016). Green scheduling of a two-machine flowshop: Trade-off between makespan and energy consumption. *European Journal of Operational Research, 248*(3), 772–788. https://doi.org/10.1016/j.ejor.2015.08.064

Meng, R., Rao, Y., & Luo, Q. (2020). Modeling and solving for bi-objective cutting parallel machine scheduling problem. *Annals of Operations Research, 285*, 223–245. https://doi.org/10.1007/s10479-019-03208-z

Meyr, H. (2002). Simultaneous lotsizing and scheduling on parallel machines. *European Journal of Operational Research, 139*(2), 277–292. https://doi.org/10.1016/S0377-2217(01)00373-3

Miettinen, K. (1998). *Nonlinear multi-objective optimization*. Springer. https://doi.org/10.1007/978-1-4615-5563-6

Moon, J., Shin, K., & Park, J. (2013). Optimization of production scheduling with time-dependent and machine-dependent electricity cost for industrial energy efficiency. *The International Journal of Advanced Manufacturing Technology, 68*, 523–535. https://doi.org/10.1007/s00170-013-4749-8

Neufeld, J., Schulz, S., & Buscher, U. (2022). A systematic review of multi-objective hybrid flow shop scheduling. *European Journal of Operational Research, 309*(1), 1–23. https://doi.org/10.1016/j.ejor.2022.08.009

Oukil, A., El-Bouri, A., & Emrouznejad, A. (2022). Energy-aware job scheduling in a multi-objective production environment – An integrated DEA-OWA model. *Computers & Industrial Engineering, 168*, 108065. https://doi.org/10.1016/j.cie.2022.108065

Pinedo, M. (2016). *Scheduling – Theory, algorithms and systems* (5th ed.). Springer. https://doi.org/10.1007/978-3-319-26580-3

Riquelme, N., Von Lücken, C., & Baran, B. (2015). Performance metrics in multi-objective optimization. In *Latin American computing conference (CLEI)* (pp. 1–11). https://doi.org/10.1109/CLEI.2015.7360024

Schulz, S., Buscher, U., & Shen, L. (2020). Multi-objective hybrid flow shop scheduling with variable discrete production speed levels and time-of-use energy prices. *Journal of Business Economics, 90*, 1315–1343. https://doi.org/10.1007/s11573-020-00971-5

Schulz, S., & Linß, F. (2020). Time-dependent emission minimization in sustainable flow shop scheduling. In *Operations Research Proceedings 2019* (pp. 583–589). https://doi.org/10.1007/978-3-030-48439-2_71

Seeanner, F., & Meyr, H. (2013). Multi-stage simultaneous lot-sizing and scheduling for flow line production. *OR-Spectrum, 35*, 33–73. https://doi.org/10.1007/s00291-012-0296-1

Tiwari, M., Chang, P., & Choudhary, A. (2015). Carbon-efficient production, supply chains and logistics. *International Journal of Production Economics, 164*, 193–196. https://doi.org/10.1016/j.ijpe.2015.02.008

T'kindt, V., & Billaut, J. (2006). *Multicriteria scheduling* (2 ed.). Springer. https://doi.org/10.1007/b106275

United Nations (UN). (2015). 2030 agenda for sustainable development. www.un.org.

Van Veldhuizen, D. (1999). *Multi-objective evolutionary algorithms: Classifications, analyses and new innovations*. Ph.D. thesis,. Dyton, Ohio: School of Engineering of the Air Force Institute of Technology.

Wang, G., Li, X., Gao, L., & Li, P. (2022). An effective multi-objective whale swarm algorithm for energy-efficient scheduling of distributed welding flow shop. *Annals of Operations Research, 310*, 223–255. https://doi.org/10.1007/s10479-021-03952-1

Wang, J., & Wang, L. (2022). A cooperative memetic algorithm with feedback for the energy-aware distributed flow-shops with flexible assembly scheduling. *Computers & Industrial Engineering, 168*(108126). https://doi.org/10.1016/j.cie.2022.108126

Weckenborg, C., Thies, C., & Spengler, T. (2022). Harmonizing ergonomics and economics of assembly lines using collaborative robots and exoskeletons. *Journal of Manufacturing Systems, 62*, 681–702. https://doi.org/10.1016/j.jmsy.2022.02.005

Wichmann, M., Johannes, C., & Spengler, T. (2019a). Energy-oriented lot-sizing and scheduling considering energy storages. *International Journal of Production Economics, 216*, 204–214. https://doi.org/10.1016/j.ijpe.2019.04.015

Wichmann, M., Johannes, C., & Spengler, T. (2019b). An extension of the general lot-sizing and scheduling problem (GLSP) with time-dependent energy prices. *Journal of Business Economics, 89*, 481–514. https://doi.org/10.1007/s11573-018-0921-9

Yenipazarli, A., & Vakharia, A. (2017). Green, greener or brown: Choosing the right color of the product. *Annals of Operations Research, 250*, 537–567. https://doi.org/10.1007/s10479-014-1781-5

Zhang, H., Zhao, F., Fang, K., & Sutherland, W. (2014). Energy-conscious flow shop scheduling under time-of-use electricity tariffs. *CIRP Annals, 63*(1), 37–40. https://doi.org/10.1016/j.cirp.2014.03.011

Zitzler, E., Knowles, J., & Thiele, L. (2008). Quality assesment of pareto set approximations. In J. Branke, K. Deb, K. Miettinen, & R. Slowiński (Eds.), *Multi-objective optimization: Interactive and evolutionary approaches* (pp. 373–404). Springer. https://doi.org/10.1007/978-3-540-88908-3.

Zitzler, E., & Thiele, L. (1998). Multi-objective optimization using evolutionary algorithms - a comparative case study. In A. Eiben, T. Bäck, M. Schoenauer, & H. P. Schwefel (Eds.), *PPSN: International conference on parallel problem solving from nature* (pp. 292–301). Springer. https://doi.org/10.1007/BFb0056872.

Zitzler, E., Thiele, L., Laumanns, M., Fonseca, C., & da Fonseca, V. (2003). Performance assessment of multi-objective optimizers: An analysis and review. *IEEE Transactions on Evolutionary Computation, 7*(2), 117–131. https://doi.org/10.1109/TEVC.2003.810758